Advanced Materials

ADVANCED MATERIALS
www.advmat.de

REVIEW

3D Printing of Magnetic Soft Materials for Functional Structures and Devices

Shouyi Yu[1] | Yingbo Yan[2] | Mei Chen[3] | Xingjian Huang[1] | Liuchao Jin[1,4] | Rong Wang[1] | Kun Zhou[3] | Qi Ge[1]

[1]Shenzhen Key Laboratory for Additive Manufacturing of High-Performance Materials, Department of Mechanical and Energy Engineering, Southern University of Science and Technology, Shenzhen, China | [2]MOE Key Laboratory of Macromolecular Synthesis and Functionalization, Department of Polymer Science and Engineering, Zhejiang University, Hangzhou, China | [3]Singapore Centre for 3D Printing, School of Mechanical and Aerospace Engineering, Nanyang Technological University, Singapore, Singapore | [4]Department of Mechanical and Automation Engineering, The Chinese University of Hong Kong, Hong Kong, China

Correspondence: Kun Zhou (kzhou@ntu.edu.sg) | Qi Ge (geq@sustech.edu.cn)

Received: 19 December 2025 | **Revised:** 11 June 2026 | **Accepted:** 18 June 2026

Keywords: 3D printing | magnetic field-assisted 3D printing | magnetic programming | magnetic soft materials

ABSTRACT

Magnetic soft materials (MSMs) have garnered widespread attention due to their advantages in wireless control, rapid response, and programmable anisotropy. Magnetically programmed MSM structures and devices have found extensive applications in fields such as miniature robots, biomedical engineering, and flexible electronics. However, their further development faces significant challenges in manufacturing, especially the need to create complex three-dimensional (3D) structures with full degrees of freedom (DoFs) magnetic programming. Traditional manufacturing approaches and 3D printing followed by post-magnetic programming face multistep workflows, limited programming freedom, and restricted filler selection. Magnetic field-assisted 3D printing (MF3DP) addresses these limitations by coupling fabrication with in situ magnetic programming, enabling the direct manufacturing of MSM structures with programmable magnetic fillers orientations. In this paper, we first introduce magnetic materials, matrix materials, and their composites, focusing on their fundamental properties and response mechanisms. Then, we review traditional manufacturing approaches and 3D printing, followed by post-magnetic programming. Next, we systematically review MF3DP technologies, providing a comprehensive discussion of magnetic field sources, field integration strategies, magnetic programming mechanisms, programming capabilities, and overall manufacturing performance. Finally, we discuss the current challenges and prospects of 3D printing of MSMs.

1 | Introduction

Magnetic soft materials (MSMs) are smart materials where magnetic particles are embedded into compliant matrices. Due to their capability of exhibiting large, rapid and reversible responses upon applied magnetic fields [1, 2], as well as the mechanical [3], electrical [4], and thermal [5] anisotropies depending on the programmed orientation of the magnetic particles, MSMs have been used to develop enormous functional structures and devices for various applications such as miniature robots [6–10], flexible sensors [11–13], property reinforced composites [14–17], and others [18, 19]. To meet these application demands, researchers have developed numerous fabrication methods, including mold casting [20–22], laser cutting [23–25], micro-assembly [26–28], and injection molding [29–31]. However, these methods typically involve multiple processes and extensive manual operations, which make them inefficient, and incapable of producing MSM structures with complex magnetic programming [32, 33]. Thus,

these traditional methods severely limit the achievable performance and functionality of MSM structures and devices.

Additive manufacturing, also known as three-dimensional (3D) printing, is an advanced manufacturing technology that creates complex 3D structures in a layer-by-layer fashion [34–36]. Due to its high design flexibility and capability of multimaterial integration, 3D printing is competent to fabricate complex 3D structures with multifunctionality [37–42]. Mainstream 3D printing methods include Fused Deposition Modeling (FDM) [43–46], Direct Ink Writing (DIW) [47–49], Inkjet [50–52], Stereolithography (SLA) [53–56], Digital Light Processing (DLP) [57–63], Two-Photon Polymerization (TPP) [64–66], and Selective Laser Sintering (SLS) [67–69]. Among them, DLP and DIW are the most commonly used methods for creating 3D structures of MSMs as they are compatible with a wide variety of polymer matrices that can incorporate magnetic particles, facilitating the fabrication of diverse functional and even multifunctional structures and devices [8, 70–73].

Applying an external magnetic field to control the orientation of magnetic particles is key to endowing fabricated magnetic structures with unique behaviors or functionalities. Here, we refer to such a process as "magnetic programming." A 3D magnetic structure without magnetic programming can be easily printed as long as the MSMs are printable. Then, the printed structure can be magnetically programmed by placing it in a pulsed magnetic field [1, 74, 75]. Here, we name such magnetically programming process as "post magnetic programming" as it is applied after the whole structure is printed. Although this approach has been used to fabricate some magnetic 3D structures [20, 23], it is incompetent to achieve complex magnetization profiles in the printed structures, which limits the performance and functionality of printed magnetic structures for advanced applications [32, 33, 76–78]. Moreover, post-magnetic programming is only applicable to hard-magnetic particles that can retain their magnetization after the external magnetic field is removed. In contrast, the structures with soft-magnetic or paramagnetic particles lose their magnetization once the field is withdrawn and therefore, cannot be programmed using this method.

To overcome those limitations, the magnetic field-assisted 3D printing (MF3DP) has been proposed. During the 3D printing process, external magnetic fields are applied through electromagnet coil, a permanent magnet, or a combination of them [32, 33, 79–81]. The applied magnetic fields can locally program the magnetic properties of printed parts during 3D printing. Therefore, we name such programming process as "in situ magnetic programming." Despite recent advances demonstrating that MF3DP has been used to successfully print numerous functional structures and devices [80, 82], substantial work still needs to be done to improve the fidelity and complexity of printed magnetic structures in terms of geometric and magnetization profiles.

Although several review articles have discussed the 3D printing of magnetic materials and have partially covered MSMs [83–89], most of them are organized from broader perspectives such as materials, processes, or applications. To the best of our knowledge, a systematic manufacturing-centered review specifically focused on MSMs remains lacking. In particular, the connections among magnetic particles, matrix materials, fabrication routes, magnetic programming strategies, and manufacturing capabilities have not been fully established within a unified framework. Clarifying these connections is essential for understanding how MSM structures can be designed, fabricated, and functionally programmed, thereby helping identify the key challenges for next-generation MSM structures and devices.

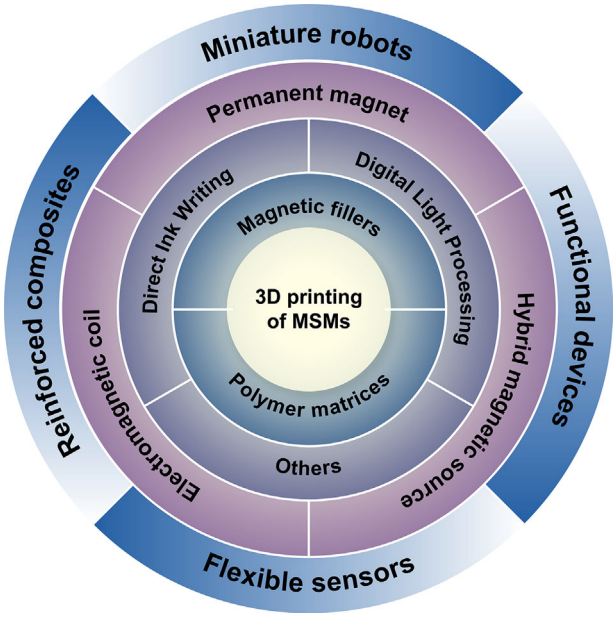

FIGURE 1 | Overview of 3D printing of MSMs: material foundations, 3D printing technologies, magnetic field sources for magnetic programming, and their relevant applications.

To address this gap, this review paper provides a systematic overview of the latest progress in 3D printing of MSMs from a manufacturing-centered perspective, highlighting the role of magnetic fields in programmed structure fabrication across different techniques and outlining potential directions for future development. Figure 1 presents an overview of 3D printing of MSMs. In this review, we first introduce the material foundations of MSMs, including the properties of magnetic particles, the classification of matrix materials, their responsive behaviors under a magnetic field, sensing mechanisms, and traditional manufacturing approaches (Section 2). We then focus on 3D printing of MSMs, beginning with strategies that rely on post magnetic programming (Section 3.1), followed by DIW- (Section 3.2) and DLP-based (Section 3.3) MF3DP. Finally, we outline future directions for MSM manufacturing, design, and functional development, namely multi-material integration, computationally guided design, and reconfigurable magnetic functionality (Section 4).

2 | Overview of MSMs and Their Traditional Manufacturing Approaches

2.1 | Classification of Magnetic Materials

Depending on magnetization characteristics, magnetic materials can be classified into three categories: hard-magnetic, soft-magnetic, and superparamagnetic materials. The key differences

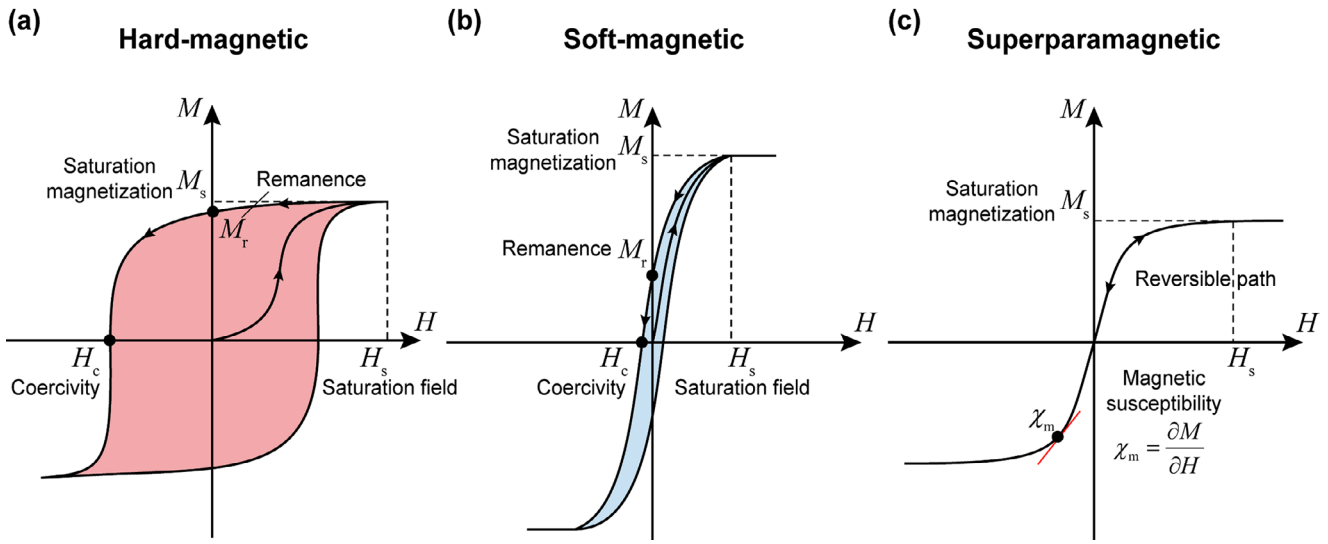

FIGURE 2 | Magnetization curves of different magnetic materials: (a) hard-magnetic materials; (b) soft-magnetic materials; (c) superparamagnetic materials.

between them can be quantified by their magnetization curves, which are presented in Figure 2.

Figure 2a presents a typical magnetization curve for a hard-magnetic material. A magnetic material is gradually magnetized as the applied magnetic field H increases. When H reaches the saturation field strength H_s, the magnetic material is magnetized at the saturated state M_s (M_s is called saturation magnetization, $M_s \leq H_s$). In engineering, the saturation magnetization is quantified by saturation magnetic flux density B_s, which can be calculated as $B_s = \mu_0 M_s$, where μ_0 is the vacuum permeability ($\mu_0 = 4\pi \times 10^{-7}$ H/m). Once H is removed, most magnetization remains in the hard-magnetic material, and remained magnetization is denoted as remanent magnetization or remanence M_r. In engineering, remanent magnetization is measured by remanent magnetic flux density B_r ($B_r = \mu_0 M_r$). To demagnetize the magnetic material, an opposite H is required to be applied. When the opposite H reaches H_c (H_c is denoted as coercivity, $H_c < H_s$), the overall magnetization of the magnetic material is reduced to zero. As listed in Table 1, typical hard-magnetic materials include $Nd_2Fe_{14}B$, $SrFe_{12}O_{19}$, and $SmCo_5$. The H_c of these hard-magnetic materials is usually greater than 400 kA/m. Since M_r and H_c are high in hard-magnetic materials, the magnetization curve of them exhibits large hysteresis.

Different from hard-magnetic materials, as shown in Figure 2b, soft-magnetic materials can be easily magnetized ($H_s \ll M_s$), and have much smaller remanence M_r. Moreover, soft-magnetic materials have weak ability to resist demagnetization. Thus, the coercivity (H_c) of them is usually less than 10 kA/m. Since M_r and H_c are low, soft-magnetic materials exhibit low hysteresis. Table 1 also lists the typical soft-magnetic materials such as Fe, Carbon Iron Powder (CIP), and FeSi.

In contrast to hard- and soft-magnetic materials, superparamagnetic materials exhibit a magnetization curve (Figure 2c) without remanence, coercivity, and hysteresis. They are highly responsive to external magnetic fields and can be rapidly magnetized and demagnetized. Compared with soft-magnetic materials, superparamagnetic materials have moderate magnetic susceptibility χ_m, which is defined as the initial slope of the magnetization curve. It is worth noting that superparamagnetic behavior is highly size-dependent, typically emerging when the particle size falls below a critical threshold, where thermal fluctuations and relaxation dominate and coercivity approaches zero. As a result, superparamagnetic particles are typically in the nanoscale range and mainly composed of iron oxide nanoparticles, such as magnetite (Fe_3O_4) and maghemite (γ-Fe_2O_3).

2.2 | Classification of Matrix Materials

Matrix material acts as a carrier where magnetic particles are embedded and provides elasticity to the corresponding MSM composite. Upon applying external magnetic fields, forces and torques acting on the individual magnetic particles generate internal stresses within the matrix material, leading to deformations of the whole composite. Thus, the extent of deformation is primarily determined by the mechanical properties of the matrix material. Nevertheless, in addition to mechanical properties, many other factors should be considered when selecting matrix materials, including compatibility with magnetic particles, processability, as well as specific functionalities for target applications.

For bio-related applications, biocompatibility is another important consideration in matrix selection. The biocompatibility of MSMs is determined not only by the matrix material itself, but also by the embedded magnetic components. On the matrix side, factors such as chemical composition, crosslinking chemistry, residual monomers or initiators, solvent environment, and long-term stability under physiological conditions may all influence cytocompatibility and safety [95, 96]. On the magnetic-component side, the particle composition, size, loading level, surface chemistry, corrosion behavior, and possible particle leakage or ion release are also important considerations [85, 97]. To improve the biocompatibility of MSMs, reported strategies have mainly included the use of more biocompatible matrices and magnetic fillers [83, 85], surface coating [8, 29] or chemical

TABLE 1 | Magnetic properties of commonly used magnetic materials [90–94].

	Material	B_s (T)	B_r (T)	H_c(A/m)	χ_m
Hard-magnetic	$Nd_2Fe_{14}B$	1.34	1.30	900k	—
	$SrFe_{12}O_{19}$	0.46	0.37	260k	—
	$SmCo_5$	0.95	0.89	680k	—
	Sm_2Co_{17}	1.15	1.09	800k	—
	$AlNiCo_5$	1.34	1.29	60k	—
Soft-magnetic	FeCrCo	1.4	1.5	60k	—
	Fe	2.16	—	4–80	10–50k
	FeSi	2.0	—	6	500–5k
	$Ni_{50}Fe_{50}$	1.4–1.6	—	4–20	70k
	$Ni_{78}Fe_{17}Mo_5$	0.65–0.82	—	0.25–0.64	100–800k
	Mn-Zn ferrite	0.36–0.5	—	10–100	500–10k
	Ni-Zn ferrite	0.25–0.42	—	14–1600	10–1k
Superparamagnetic	Fe_3O_4 nanoparticles	0.02–0.65	—	—	0.003–0.007

modification [98] of magnetic particles to reduce direct exposure and improve interfacial stability, and encapsulation [99, 100] of the magnetic phase to minimize leakage and enhance long-term stability in biological environments.

The matrix materials used in MSMs can be broadly classified into passive and active matrices according to whether they only provide mechanical compliance or can also actively respond to external physical stimuli other than magnetic fields. Traditionally, matrix materials such as elastomers and gels are considered passive matrices, which mainly provide elasticity to the composites, while the actuation of the composites arises from the embedded magnetic particles under applied magnetic fields. In contrast, active matrices refer to soft matrix materials that can actively respond to other physical fields, thereby introducing additional actuation or shape-fixing functionalities into the composite system. Recently, active materials such as shape memory polymers and liquid crystal elastomers have also been used as matrix materials, which impart multifunctionality to magnetic soft materials so that they exhibit not only magnetic actuation but also thermal or photothermal actuation. In the following sections, we discuss some commonly used passive and active matrix materials.

Among various matrix materials, thermosetting silicone elastomers are chemically crosslinked polymer networks with low crosslinking density (Figure 3a), and have been the most widely used for the fabrication of MSMs owing to their broad commercial availability. Representative products include Sylgard 184 (Dow Chemical), Ecoflex (Smooth-On, Inc), and Elastosil (Wacker Chemie AG). They are addition-curing type silicone elastomers whose curing process can be accelerated by heating in the presence of platinum-based catalysts. Unless heavily loaded, the magnetic particles can be easily mixed into the uncured silicone resin prior to catalyst addition. Then, the mixture can form desired shapes through casting, molding, or printing, and the liquid mixture with a catalyst solidifies upon thermal curing.

Thermoplastic elastomers such as thermoplastic polyurethane (TPU) have also been used as matrix materials for preparing MSM composites. Different from chemically crosslinked silicone elastomers, thermoplastic elastomers are block copolymers with rigid crystalline segments that physically crosslink flexible segments (Figure 3b). Thermoplastic elastomers melt upon heating, allowing magnetic particles to be mixed into the molten thermoplastic elastomers through melt blending in a twin-screw extruder. Then, the molten blends can form desired shapes through manufacturing processes such as extrusion, injection, and compression molding. Upon cooling, the thermoplastic elastomer solidifies again, and the material regains its mechanical properties.

Gels are another type of matrix materials which have been widely used. Different from elastomers, gels are semisolids composed of loosely crosslinked polymer networks where liquid solvents are entrapped (Figure 3c). Among all gels, hydrogels are the most widely used and are composed of hydrophilic polymer networks containing a large amount of water. Due to the excellent biocompatibility, hydrogels with embedded magnetic particles have shown great potential in biomedical applications [101–103]. The hydrogels used for hosting magnetic particles include synthetic polymers such as polyacrylamide [104–106], poly(vinyl alcohol) [107–110], and poly(N-isopropylacrylamide) [103, 111, 112], and natural polysaccharides such as alginate [113, 114], scleroglucan [115], and carrageenan [116–119].

Passive matrices offer elasticity to the MSMs, which deform reversibly under applied magnetic fields. However, the deformation cannot be maintained after the removal of the applied magnetic fields. Thus, in order to maintain the deformed shape without continuously applying magnetic fields, active materials such as shape memory polymers (SMPs) [120–123] and liquid crystal elastomers (LCEs) [124, 125] have been used as matrix materials for MSMs. As shown in Figure 3d, SMPs exhibit shape memory (SM) behavior through a SM cycle: it is deformed at high temperature (T_h), which is above its transition temperature

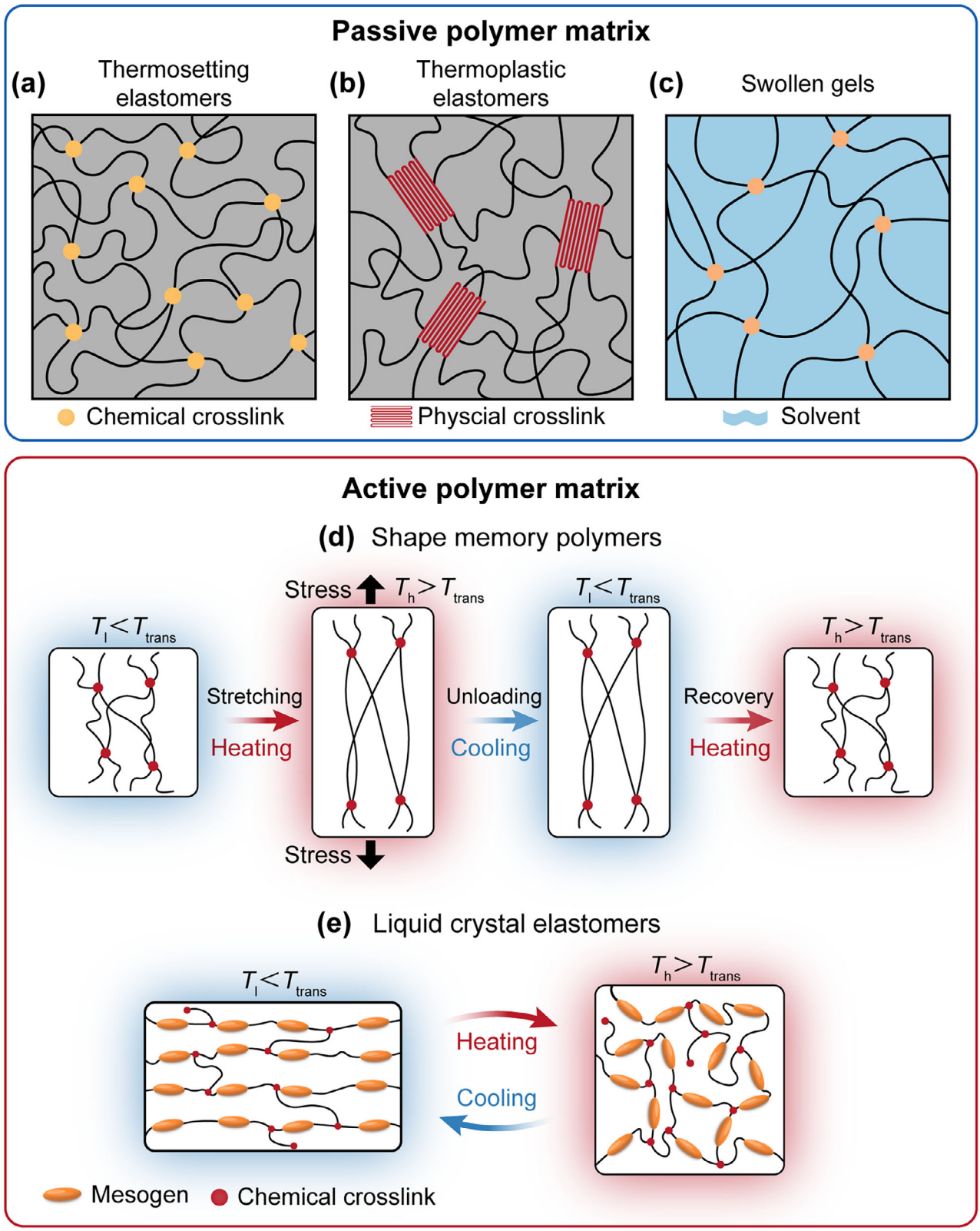

FIGURE 3 | Classification of polymer matrices used in MSMs. (a–c) Passive polymer matrices, including (a) thermosetting elastomers, (b) thermoplastic elastomers, and (c) solvent-swollen gels. (d, e) Active polymer matrices, including (d) shape memory polymers, which undergo thermally induced temporary shape fixation and recovery around a transition temperature T_{trans}, and (e) liquid crystal elastomers, which respond to thermal stimuli via reversible mesogen alignment transitions.

(T_{trans}: glass transition temperature for amorphous SMP and crystallization temperature for crystalline SMP); the SMP sample is cooled to a low temperature state (T_l) while keeping the external load; after removing the external load, the temporary shape is fixed; the SMP recovers to its original shape. If hard- or soft-magnetic particles are embedded into the SMP matrix, the MSM composite can be deformed by an applied magnetic field when it is heated at T_h. The deformation can be maintained if even the magnetic field is removed when the SMP is cooled down to T_l. When superparamagnetic particles are embedded into the SMP matrix, the shape recovery of the SMP can be triggered by applying alternating magnetic fields.

Liquid crystal elastomers (LCEs) are another type of thermo-responsive active materials that have been used as matrices for MSMs. As illustrated in Figure 3e, within the loosely linked polymer network, there are rod-like rigid molecules called mesogens, which are covalently attached to the network. At low temperature (T_l), the LCE is in the nematic state, in which the mesogens can be programmed to align along a common direction. Upon heating to a high temperature (T_h), which is above the transition temperature (T_{trans}), the mesogens undergo a transition from the ordered nematic state to the randomly distributed isotropic state. Accompanied by this transition, contraction occurs in the LCE sample. When cooled back to T_l, the LCE returns to the nematic state and recovers its original length. Therefore, LCEs exhibit reversible actuation upon heating and cooling. When superparamagnetic particles are embedded into the LCE matrix, such reversible actuation can be remotely controlled by applying alternating magnetic fields.

2.3 | Responsive Behaviors of MSMs Under Magnetic Fields

Hard-magnetic materials such as $Nd_2Fe_{14}B$, $SrFe_{12}O_{19}$, and $SmCo_5$ are characterized by high coercivity, which allows them to be relatively insensitive to external magnetic fields, and more resistant to demagnetization when compared with soft-magnetic materials. Hence, hard-magnetic materials can maintain their high remanent magnetization even under external magnetic fields as long as they are below the coercivity of the hard-magnetic materials.

As shown in Figure 4a, due to the dipole moment resulting from the remanent magnetization, the magnetic torque of a hard-magnetic particle can be readily achieved when it is placed in a spatially uniform magnetic field. Once the hard-magnetic particles with remanent magnetization are embedded into an elastic matrix, the magnetic torques generated from a uniform magnetic field would lead to bending actuation of the matrix. Figure 4b illustrates an elastic beam where the magnetization profile of the hard-magnetic particles is along the longitudinal direction of the beam. Under a spatially uniform magnetic field perpendicular to the beam, the embedded hard-magnetic particles tend to align their remanent magnetization with the applied magnetic field due to the magnetic torques, which results in bending actuation of the beam. As shown in Figure 4c, under spatially nonuniform magnetic fields, both magnetic torque and force act on the hard-magnetic particle, which tends to rotate and move toward the direction where the field strength increases. Accordingly, for the magnetization profile illustrated in Figure 4b,d, the magnetic force and magnetic torque act cooperatively, leading to a larger bending deformation in the nonuniform field than in the uniform field. However, this enhancement is not universal. Depending on the magnetization profile, field distribution, and boundary conditions, the effects of magnetic torque and force may also compete with each other. For example, if the magnetization directions in the two halves of the beam are reversed compared with the configuration illustrated in Figure 4b,d, the magnetic force may weaken the overall deformation or even dominate over the magnetic torque, thereby reversing the deformation.

Compared with hard-magnetic materials, soft-magnetic materials such as Fe, FeSi, and $Ni_{50}Fe_{50}$ are characterized by lower remanence and coercivity but higher magnetic susceptibility and saturation magnetization (Figure 2b). Thus, soft-magnetic materials are easily magnetized, but also easily demagnetized by relatively weak magnetic fields. When a magnetic field is applied to a spherical soft-magnetic particle that is magnetically isotropic, there is no torque but only force acting on the particle (Figure 5a), since the induced magnetic moment is always aligned with the applied field. Therefore, it is easier to generate elongation or compression (Figure 5b) than bending in an MSM composite where spherical soft-magnetic particles are embedded. To produce magnetic torques on soft-magnetic materials, magnetic anisotropy needs to be introduced by either forming anisotropic soft-magnetic particles with nonspherical shapes (e.g., rods, spheroids, platelets) or chains of isotropic particles to generate magnetic asymmetry (Figure 5c). As a result, the application of a magnetic field leads to bending actuation of the MSM composite with embedded chains of isotropic soft-magnetic particles on which magnetic torques act (Figure 5d).

Superparamagnetic materials such as iron oxide nanoparticles are characterized by the near absence of remanence and coercivity as well as high magnetic susceptibility. Similar to soft-magnetic materials, superparamagnetic materials cannot produce magnetic torques if the particles are not imparted with magnetic anisotropy. Moreover, as the superparamagnetic nanoparticles tend to aggregate, the maximum concentration of superparamagnetic nanoparticles in the polymer matrix is much lower than that of hard- or soft-magnetic microparticles. Due to the above limitations, superparamagnetic nanoparticles are not ideal for producing actuation for MSMs but have a unique capability of converting electromagnetic energy into heat through thermal relaxation under alternating magnetic fields, which is more effective and efficient than soft- or hard-magnetic microparticles that mainly generate heat through magnetic hysteresis. Therefore, when superparamagnetic nanoparticles are embedded into a thermally responsive polymer matrix, such as SMPs, LCEs, or others, the shape changes of these MSM composites can be achieved by applying alternating magnetic fields. As shown in Figure 6a, an SMP MSM composite recovers from the bent temporary shape to its straight original shape due to internal heating through the released energy from the superparamagnetic nanoparticles under an alternating magnetic field. Figure 6b shows that reversible actuation of an LCE MSM composite with superparamagnetic nanoparticles can be readily achieved by tuning the alternating magnetic field.

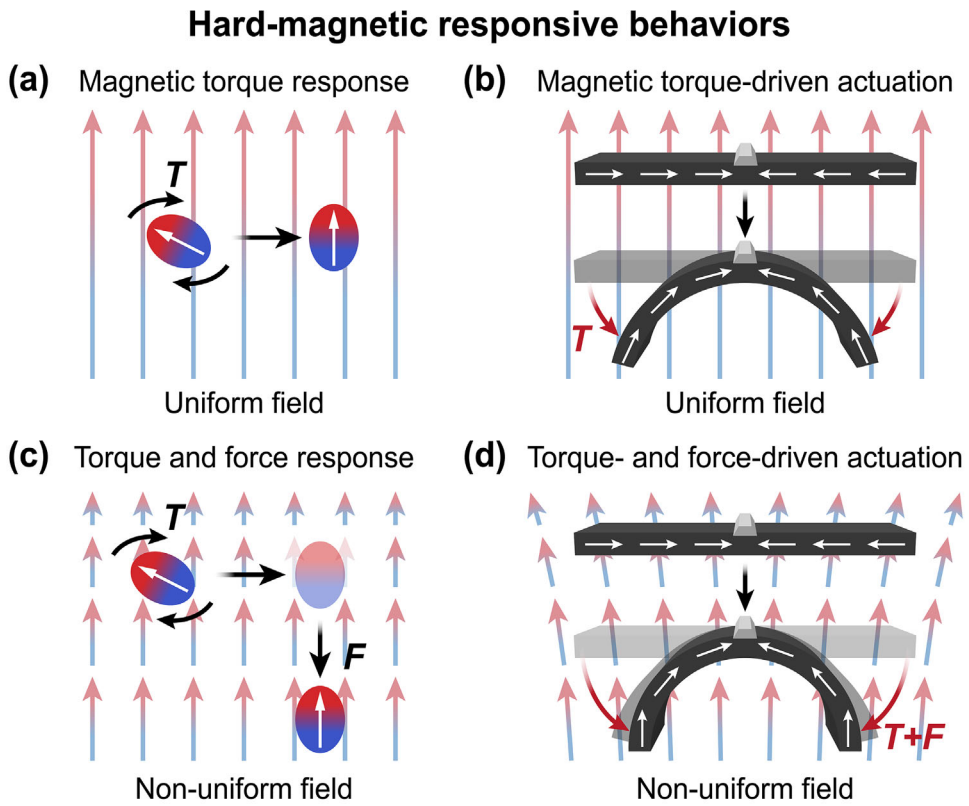

FIGURE 4 | Magnetic field responsive behaviors of hard-magnetic particles and MSM composites. In uniform magnetic fields, hard-magnetic particles with remanent magnetization generate magnetic torques, enabling (a) particle rotation and (b) torque-driven bending of the MSM composite. In non-uniform magnetic fields, both magnetic torque and force act on the hard-magnetic particles, resulting in (c) combined torque and force response and (d) enhanced deformation of the MSM composite.

2.4 | Sensing Mechanisms of MSM-Based Sensors

Beyond actuation, the coupled magneto-mechanical response of MSMs can also be exploited for sensing [11, 99, 100, 126–129]. In this case, external mechanical stimuli, such as pressure, shear, bending, or compression, first perturb the internal magnetic state of the material, and the resulting magnetic variation is then converted into a measurable electrical signal. From this perspective, MSM-based sensing can be regarded as the reverse use of magneto-mechanical coupling: rather than using magnetic fields to drive deformation, deformation or displacement is used to reconfigure the magnetic state and generate readable outputs. As illustrated in Figure 7, two representative sensing mechanisms are commonly adopted in MSM-based sensors, namely Hall-effect-based sensing and electromagnetic-induction-based sensing.

In Hall-effect-based sensing, deformation or displacement of the magnetic component alters the local magnetic field around the Hall sensor, and the resulting magnetic variation is then read out by the sensor. In practical devices, the Hall sensor internally converts the Hall voltage into calibrated magnetic-field components, such that the quantities directly used for subsequent signal processing are typically the local magnetic flux density components B_x, B_y, and B_z, rather than the raw Hall voltage itself. This mechanism has been widely used in magnetic soft tactile sensors, where force-induced deformation modifies the magnetic field distribution beneath a flexible support layer and enables the sensing of normal, shear, or multidirectional loads [128, 129]. In particular, by appropriately designing the magnetic-field distribution of the magnetic component, Hall-based MSM sensors can further achieve decoupled sensing of two-axis [128] or even three-axis [129] force components.

In electromagnetic-induction-based sensing, the governing mechanism is flux variation through a coil. Under applied loading, deformation of a hard- or soft-magnetic MSM structure alters the magnetic field distribution and thereby changes the magnetic flux threading the surrounding or integrated coil. According to Faraday's law, this time-varying magnetic flux induces an electromotive force, producing an electrical output without requiring an external power source. Compared with Hall-effect-based sensing, the directly accessible signal in this route is usually the induced voltage V_i associated with overall flux variation, rather than a spatially resolved magnetic-field vector. Therefore, existing devices are mainly used to detect overall strain- or stress-related changes through electrical signal variations, rather than anisotropic sensing of different loading conditions [11, 99, 100, 126, 127]. Owing to the simple readout requirement that only a nearby coil is needed for signal collection, this sensing route is particularly attractive not only for stress/strain sensing [11, 126, 127], but also for biomedical devices with integrated sensing capability, such as magnetoelastic vascular grafts [99] and magnetoelastic stents [100].

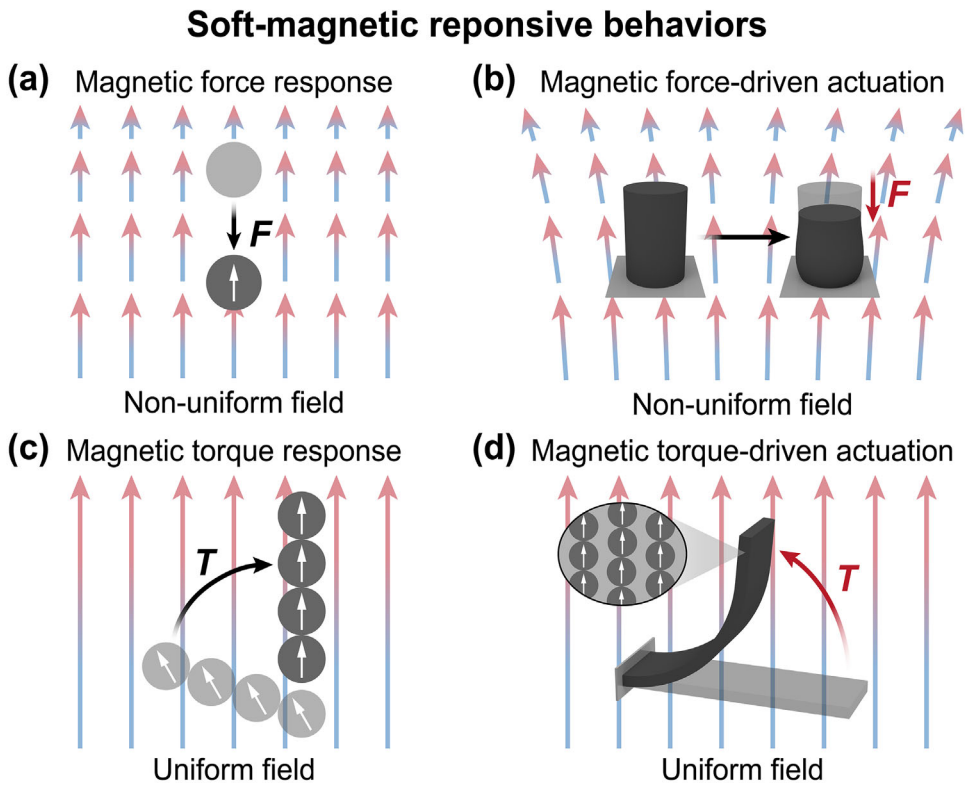

FIGURE 5 | Magnetic field responsive behaviors of soft-magnetic particles and MSM composites. In non-uniform magnetic fields, soft-magnetic particles experience magnetic force due to field gradients, causing (a) particle displacement and (b) force-driven actuation (e.g., shortening) of isotropic soft-magnetic materials. In uniform magnetic fields, anisotropic particles (e.g., chains of isotropic particles) generate magnetic torque, enabling (c) rotational alignment and (d) torque-driven deformation of the MSM composite.

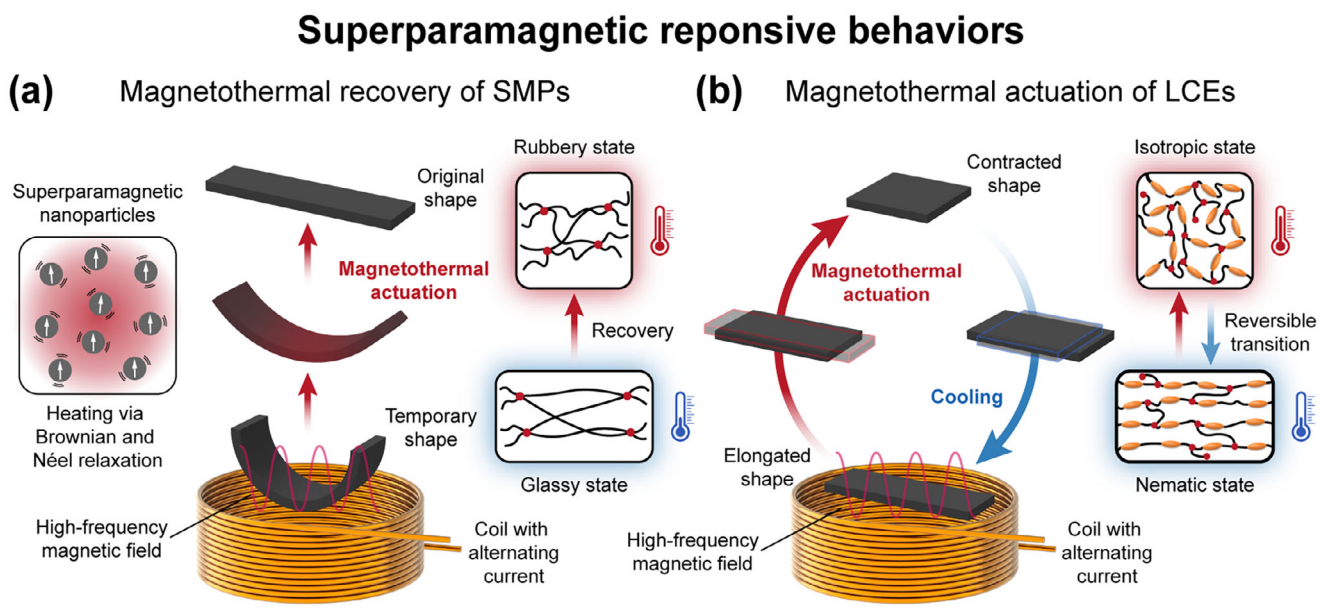

FIGURE 6 | Magnetic field responsive behaviors of superparamagnetic nanoparticle embedded MSM composites. (a) Superparamagnetic SMP-based MSM composites: magnetothermal actuation enables recovery from a temporary shape to the original shape through thermally induced glass transition. (b) Superparamagnetic LCE-based MSM composites: magnetothermal actuation and cooling enable reversible deformation through thermally induced phase transitions.

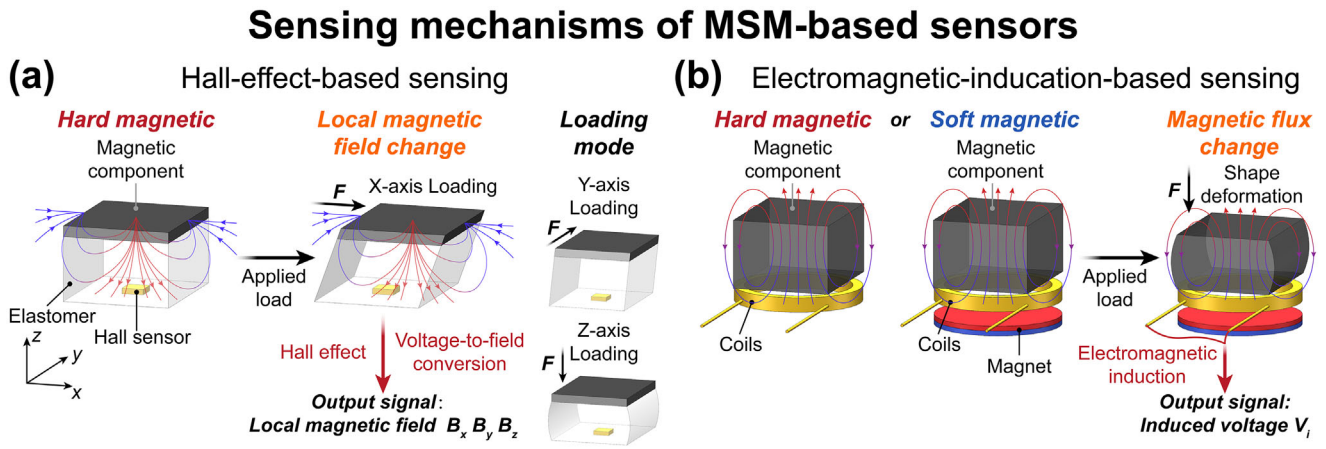

FIGURE 7 | Sensing mechanisms of MSM-based sensors. (a) In Hall-effect-based sensing, deformation or displacement of the hard-magnetic component changes the local magnetic field around the Hall sensor, which is read out as B_x, B_y, and B_z. (b) In electromagnetic-induction-based sensing, deformation of hard- or soft-magnetic components changes the magnetic flux through the coil and generates an induced voltage V_i.

Although the electrical readout mechanisms are different, both sensing routes share the same physical origin: mechanical loading modifies the magnetic state of the MSM, and the resulting magnetic variation is converted into an electrical signal through an appropriate transduction unit. This also implies that the sensing performance is not governed solely by the readout element but is strongly influenced by the magnetic microstructure established during fabrication. In particular, the type of magnetic materials, particle content, spatial distribution, and alignment state all determine how the local magnetic field or magnetic flux evolves under deformation. For Hall-effect-based sensing, these structural features mainly affect the magnitude and distribution of the local magnetic field, thereby influencing sensitivity, directional selectivity, and decoupling capability. For electromagnetic-induction-based sensing, the orientation of magnetic particles and the spatial distribution of different magnetic particles within the structure may produce different voltage outputs under different loading conditions, thereby endowing the sensor with anisotropic sensing capability.

2.5 | Traditional Approaches for Manufacturing MSMs Structures

As summarized in Figure 8, traditional approaches used to manufacture MSM structures can be broadly categorized into four types: mold casting [10, 11, 20–22, 75, 128, 130, 131], laser cutting [23–25, 76, 132, 133], micro-assembly [26–28, 77, 134], and injection molding [29–31, 135, 136].

Among them, mold casting remains the most straightforward approach. Figure 8a presents the steps of mold casting, where a liquid precursor containing magnetic particles is poured into a mold and then cured into a solid structure, whose geometry is determined by the mold. Subsequently, magnetic programming of the MSM structure can be realized with the aid of a template. Due to its simplicity and low cost, mold casting has been widely used to fabricate miniature soft robots [20, 22], metamaterials [21, 130], and flexible sensors [11, 128].

Laser cutting is another widely used approach to fabricate MSM structures. As shown in Figure 8b, this approach generates 2D MSM patterns by using a high-power laser to cut MSM thin sheets. Through template-assisted magnetic programming, the 2D MSM patterns with spatially variable magnetic profiles can be readily achieved. Due to its capability of achieving 2D MSM patterns with complex geometry and high resolution, laser cutting is particularly suitable for producing 2D miniature soft robots [23, 132, 133] and origami structures [24, 25], where high-resolution patterns with complex designs are essential.

The MSM structures fabricated through mold casting and laser cutting are 2D films or sheets with designed patterns. To achieve 3D MSM structures, micro-assembly is adopted. As shown in Figure 8c, small magnetic cubic voxels (typically ranging from tens of micrometers to a few millimeters) are first achieved through mold casting or laser cutting, and each individual magnetic voxel is magnetically programmed. Then, these small magnetic voxels are assembled into larger 3D constructs. This approach enables a high degree of design freedom through locally defining the magnetization as well as the mechanical property of each voxel. However, the method is technically demanding. Assembling sub-millimeter components requires intensive manual handling, which makes the process laborious and inconsistent. Even so, thanks to the advantages mentioned above, this approach has been used to fabricate miniature soft robots with diverse functions such as targeted drug delivery [26], complex shape-morphing [77], multimodal motion [27], liquid sampling [28], and flow-powered locomotion [134].

Injection molding is another casting-based approach. As shown in Figure 8d, in this process, an MSM precursor is injected into a tubular mold (like helical or linear shapes). The MSM precursor is then cured through UV irradiation or heating to form a 3D solid structure whose geometry is defined by the tubular mold. Then, the 3D structure is magnetically programmed within the mold. Afterward, the MSM 3D structure is achieved after demolding, which is realized by cutting open the tubular mold. Injection molding is an efficient and relatively low-cost process,

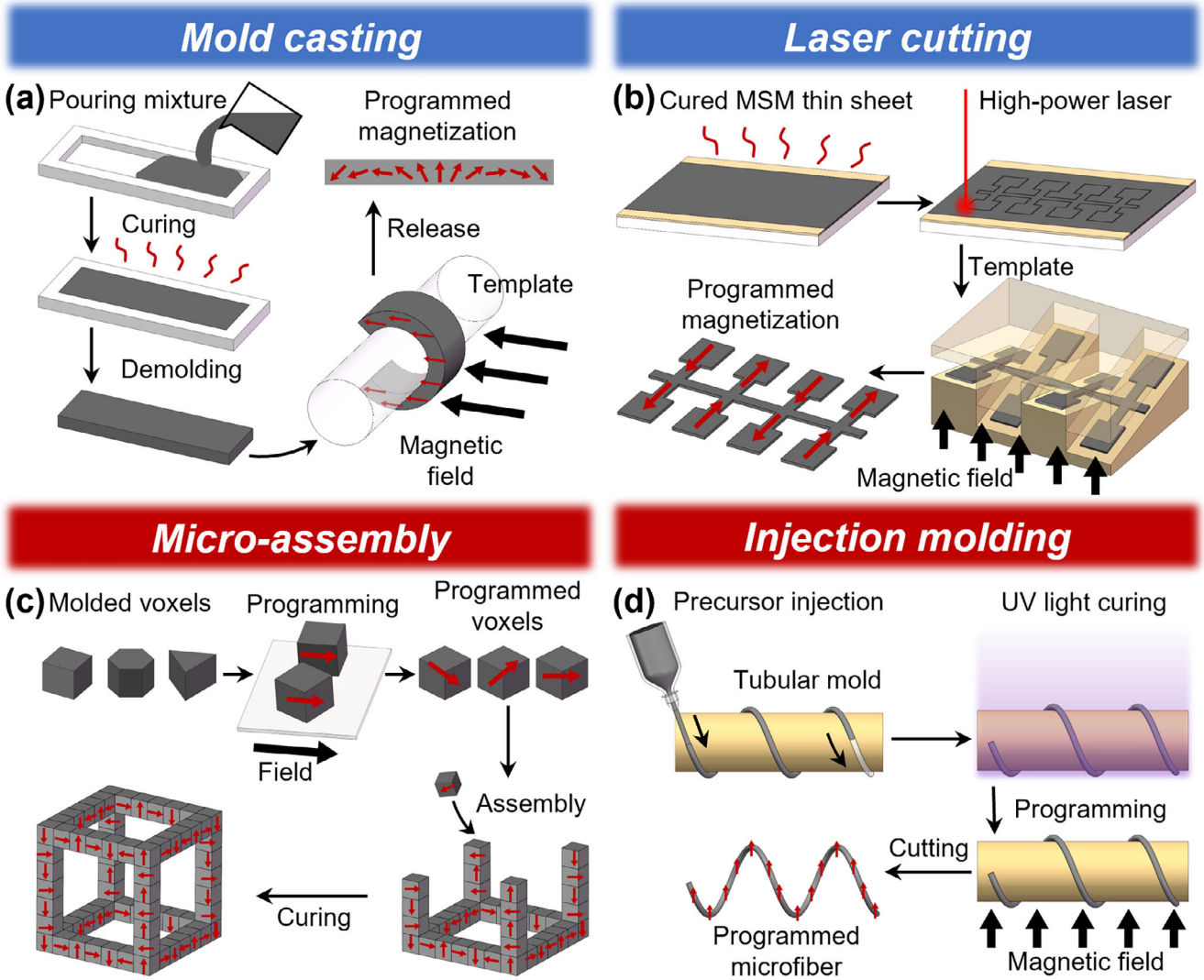

FIGURE 8 | Traditional approaches for manufacturing MSM structures, including (a) mold casting, (b) laser cutting, (c) micro-assembly, and (d) injection molding.

particularly suitable for producing slender 3D MSM structures with complex shapes. Therefore, it is widely used to fabricate helical microfibers that can serve as microswimmers in fluidic environments [20, 30, 135].

Figure 9 compares the above four traditional approaches under a unified set of capability criteria, including geometric complexity (Geo. Comp.), resolution, process simplicity (Proc. Simp.), economy, as well as magnetic programming capability (MP Cap.). Here, in the Structural Configuration/Geo. Comp. dimension, "3D" refers to structures with regular geometric shapes or relatively simple three-dimensional features, such as solid cuboid-like geometries or simple helical forms, whereas "complex 3D" refers to structures with higher geometric and topological complexity, such as hollow lattice architectures represented by octet-truss structures or complex geometries represented by triply periodic minimal surface (TPMS) structures. As summarized in Figure 9, the traditional approaches for manufacturing MSM structures exhibit distinct advantages and limitations across these dimensions, and a clear trade-off can be observed between geometric complexity and process simplicity.

Mold casting is the simplest and most cost-efficient approach, suitable for producing 2D to simple 3D structures from the centimeter to millimeter scales, but it offers limited freedom in magnetization programming and structural complexity. Laser cutting, by contrast, enables rapid and precise generation of intricate 2D geometries without mold design, making it advantageous in process simplicity. However, its scope remains restricted to planar configurations, and the requirement of specialized laser systems makes it relatively costly compared with other approaches. Micro-assembly stands out for its ability to construct complex 3D architectures with discrete magnetization profiles, even integrating multiple materials, yet its heavy reliance on manual intervention renders the process time-consuming, technically demanding, and less cost-efficient. Injection molding is particularly effective for producing filamentary MSMs such as helical microfibers, balancing relatively low cost and reproducibility, though its process simplicity remains modest. Overall, this comparison shows that traditional MSM manufacturing methods remain useful for selected structures and applications, but their capability boundaries also clearly motivate the development of more advanced manufacturing routes for MSM structures

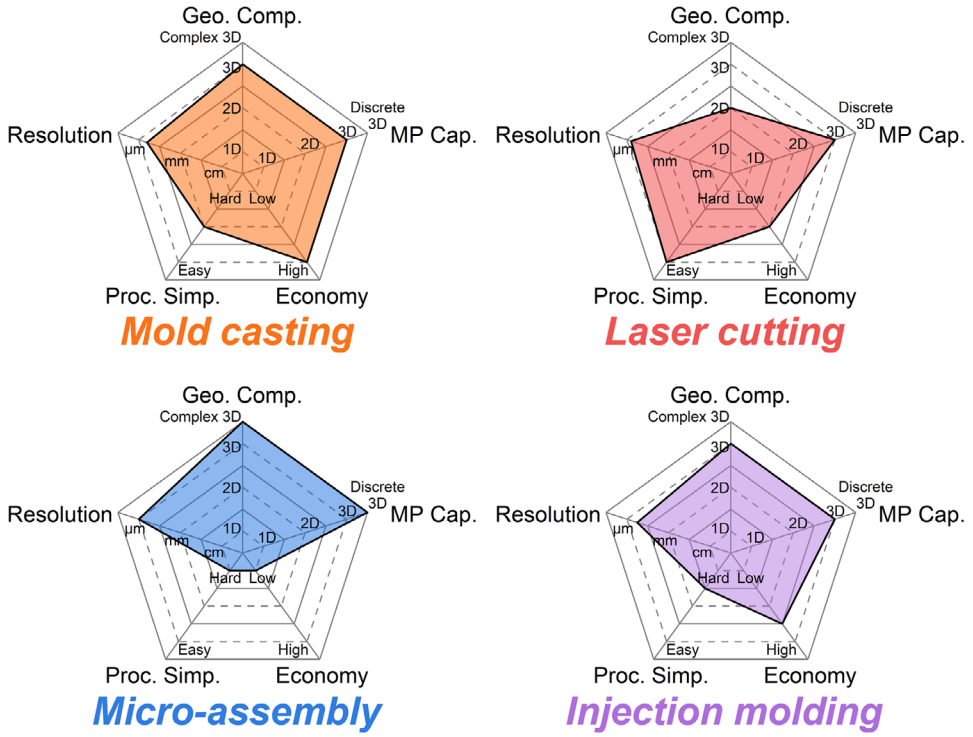

FIGURE 9 | Comparison of the manufacturing capability of traditional approaches for MSM structures. The radar plots compare geometric complexity (Geo. Comp.; 1D to complex 3D), resolution (cm to μm), process simplicity (Proc. Simp.; hard to easy), economy (low to high), and magnetic programming capability (MP Cap.; 1D to discrete 3D).

with higher geometric complexity and more integrated magnetic programming.

3 | 3D Printing of MSM Structures

3.1 | 3D Printing of MSM Structures Followed by Post Magnetic Programming

Compared with the above traditional approaches, 3D printing is an advanced manufacturing technology that can readily fabricate complex 3D structures through a single step, thereby enabling diverse MSM applications spanning miniature robotics, flexible sensors, structural materials, and functional devices. As illustrated in Figure 10a, 3D printing has been used to fabricate MSM structures once the feedstock materials (filament, ink, or resin) are loaded with magnetic particles. Once an MSM structure is printed, post-magnetic programming needs to be applied to define the magnetic profile within the 3D-printed structure. Commonly used 3D printing techniques include FDM [137–141], SLS [12, 127, 142–144], TPP [9, 145–148], DIW [72, 149–158], and DLP [8, 16, 17, 70, 71, 73, 159–163].

As shown in Figure 10b, Cao et al. employed FDM with thermoplastic rubber and carbonyl iron particles to fabricate biomimetic magnetic actuators capable of reversible flower- and butterfly-inspired shape transformations under magnetic fields [138]. In Figure 10c, Wu et al. employed SLS to fabricate NdFeB/TPU-based liquid metal-coated magnetoelectric sensors with complex MSM architectures that are capable of multidirectional force detection and deformation response [127]. In Figure 10d, Ceylan et al. fabricated a biodegradable microswimmer via TPP, which is magnetically driven for in vivo drug delivery and theranostic applications [145].

In Figure 10e, Li et al. used multimaterial cryogenic DIW to fabricate an MSM turbine robot that can transport a capsular-like cargo through a Y-shaped tube by steering its rotational axis and switching between sweeping and dragging modes [149]. In Figure 10f, Zhang et al. used coaxial DIW technology to manufacture a magnetic-mechanical-electrical gripper that can perform various tasks, including object grasping, identification, transferring, and releasing [150]. In Figure 10g, Hwang et al. used DIW technology to manufacture an MSM capsule that can undergo shape programming and recovery with local shape-morphing capability, which allows it to open its cap and release liquid on-demand in response to NIR irradiation [152].

In Figure 10h, Huang et al. used DLP technology to manufacture an MSM gear that can rotate under an alternating magnetic field, with its angular velocity increasing as the magnetic field frequency rises [70]. In Figure 10i, Zhou et al. used DLP technology to manufacture a jellyfish-shaped MSM robot that can swim by flapping its tentacles in an alternating magnetic field, achieving underwater locomotion [71]. In Figure 10j, Su et al. used DLP technology to manufacture a modularized microrobot that can be magnetically navigated through a bile duct model, performing tasks such as targeted cell delivery, on-demand CS module release, and MA module retrieval [8].

Even though it has achieved numerous demonstrations and applications, the approach that fabricates MSM structures through 3D

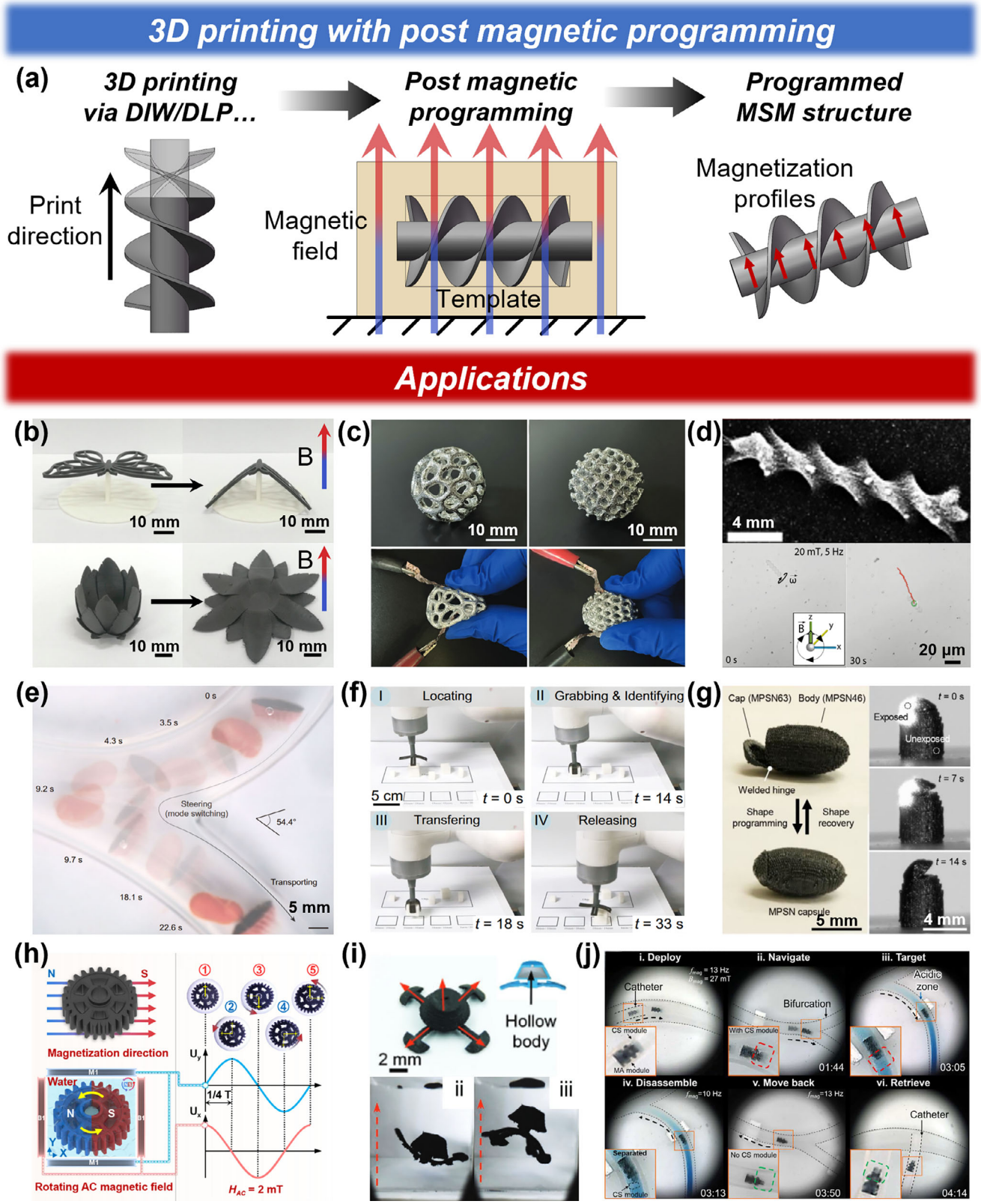

FIGURE 10 | 3D printing of MSM structures with post magnetic programming for various applications. (a) Schematic of 3D printing with post-magnetic programming. (b) FDM-based biomimetic magnetic actuators inspired by flower blooming and butterfly flapping. (Reproduced with permission [138]. Copyright 2021, American Chemical Society). (c) SLS-fabricated liquid metal-coated magnetoelectric sensors with force detection and deformation response. (Reproduced with permission [127]. Copyright 2024, Wiley-VCH). (d) TPP-fabricated biodegradable, magnetically powered microswimmer for targeted drug delivery. (Reproduced under the CC BY 4.0 license [145]. Copyright 2019, The Authors, published by Springer Nature). (e) Cryogenic DIW-fabricated MSM turbine robot for transporting cargo through a Y-shaped tube. (Reproduced under the CC BY-NC-ND 4.0 license [149]. Copyright 2025, The Authors, published by Springer Nature). (f) Coaxial DIW-fabricated MME gripper for object grasping, identification, transfer,

printing followed by post magnetic programming has obvious constraints. As the magnetic programming can only be applied after the whole MSM structure is printed, it is incapable of defining local magnetization within a structure. More importantly, such post-magnetic programming can only be applied to MSM structures loaded with hard-magnetic particles, which can maintain their magnetization after the removal of magnetic fields. In contrast, the post-magnetic programming is not applicable to the MSM structures with soft-magnetic or paramagnetic particles, which lose their magnetization once the magnetic field is withdrawn. To overcome the constraints, the magnetic field-assisted 3D printing (MF3DP) has been proposed to realize in situ magnetic programming by applying a magnetic field during the 3D printing process. To date, the 3D printing technologies suitable for MF3DP mainly include DIW and DLP. Therefore, the following section reviews the recent progress on DIW- and DLP-based MF3DP.

3.2 | Magnetic Field Assisted DIW 3D Printing

DIW is a nozzle extrusion-based 3D printing technique that forms 3D structures by extruding viscoelastic inks onto a printing platform. The success of DIW printing relies on the shear-thinning behavior of the viscoelastic inks. Under high shear stress during extrusion, the ink undergoes a sharp decrease in both modulus and viscosity, allowing it to flow smoothly through the nozzle. After extrusion, the ink rapidly recovers its high elastic modulus, facilitating shape retention of the printed structures. To print magnetic structures through DIW, magnetic particles need to be homogeneously mixed into the inks. To precisely define the orientation of magnetic particles during the 3D printing process, magnetic fields should be added to the DIW printer. As shown in Figure 11, depending on the position where the magnetic fields are applied, the DIW-based MF3DP can be categorized as: magnetic programming on ink (Figure 11a–c) and magnetic programming on printed filament (Figure 11d,e).

Figure 11a illustrates a typical DIW-based MF3DP system where magnetic programming occurs on ink. An electromagnetic coil is placed around the dispensing nozzle to generate a magnetic field along (or opposite to) the flow direction of the ink, which aligns the initially randomly oriented magnetic particles. Shear-thinning behavior makes the ink recover to its high viscosity after extrusion, so that the aligned magnetic particles are well preserved within the printed filaments or structures. To prevent the magnetic field from affecting the magnetic programming profiles of the already printed structures, magnetic shielding is placed beneath the field source. Once a magnetic soft structure is printed, further thermal or UV curing can permanently fix the alignment of the magnetic particles within the printed structure. Since the magnetic particles are aligned along the extrusion (or filament) direction, the magnetic programming profiles within the printed structure can be easily programmed by altering the local directions of the printed filaments.

In Figure 11a, the magnetic field is generated by an electromagnetic coil, enabling real-time modulation of the magnetic field and dynamic switching of the alignment direction of the magnetic particles within the filament (either aligned with or opposite to the printing direction). However, electromagnetic coils suffer from the overheating issue during prolonged operation, which limits their applicability for long-duration 3D printing processes. As shown in Figure 11b, using a permanent magnet avoids the overheating issue, although the direction of the magnetic field cannot be dynamically switched. Additionally, rather than magnetic programming only along the filament direction through uniaxial magnetic fields in Figure 11a,b, the application of multi-axial magnetic fields enables magnetic programming inside the printed filament just extruded from the printing nozzle. As shown in Figure 11c, a multi-axial magnetic field is generated by orthogonal electromagnetic coils, which are localized at the nozzle tip. This multi-axial magnetic field ensures that the programming direction of the magnetic particles is determined solely by the direction of the applied magnetic field rather than the printing direction.

Compared with the DIW-based MF3DP with magnetic programming on ink, which requires tremendous efforts to add permanent magnets or electromagnetic coils to the printing nozzle, magnetic programming on filament can be simply achieved by placing a permanent magnet or parallel permanent magnets near the freshly extruded filament to realize in situ magnetic programming. (Figure 11d,e). Since the extruded filament has a much higher viscosity than the ink during extrusion, programming the magnetic particles within the extruded filament becomes difficult. To ensure that magnetic particles within the printed filaments can be effectively magnetically programmed, soft-magnetic or superparamagnetic materials are used as magnetic particles for preparing the magnetic inks, as they are easier to align with magnetic fields.

Moreover, in situ curing (usually UV curing) is applied to the printed filament, which has been magnetically programmed to fully fix the orientation of the magnetic particles embedded in the filament and avoid them being reoriented by magnetic programming on the subsequent segment of the filament. Additionally, to mitigate the forces exerted on the magnetic particles which are resulted from the non-uniform magnetic field generated by a stationary permanent magnet, it is necessary to adjust the distance between the programming magnet and the printed filament or rotate the permanent magnet at high speed to create a nearly uniform magnetic field [164].

and releasing. (Reproduced under the CC BY 4.0 license [150]. Copyright 2023, The Authors, published by Springer Nature). (g) DIW-fabricated MSM capsule with shape programming and on-demand liquid release via NIR irradiation. (Reproduced with permission [152]. Copyright 2025, Wiley-VCH). (h) DLP-fabricated MSM gear with rotation under an alternating magnetic field. (Reproduced under the CC BY 4.0 license [70]. Copyright 2023, The Authors, published by IOP Publishing). (i) DLP-fabricated jellyfish-shaped MSM robot for underwater locomotion. (Reproduced with permission [71]. Copyright 2022, Wiley-VCH). (j) DLP-fabricated modularized microrobot for magnetic navigation, cell delivery, and module release/retrieval. (Reproduced under the CC BY-NC 4.0 license [8]. Copyright 2023, The Authors, published by American Association for the Advancement of Science).

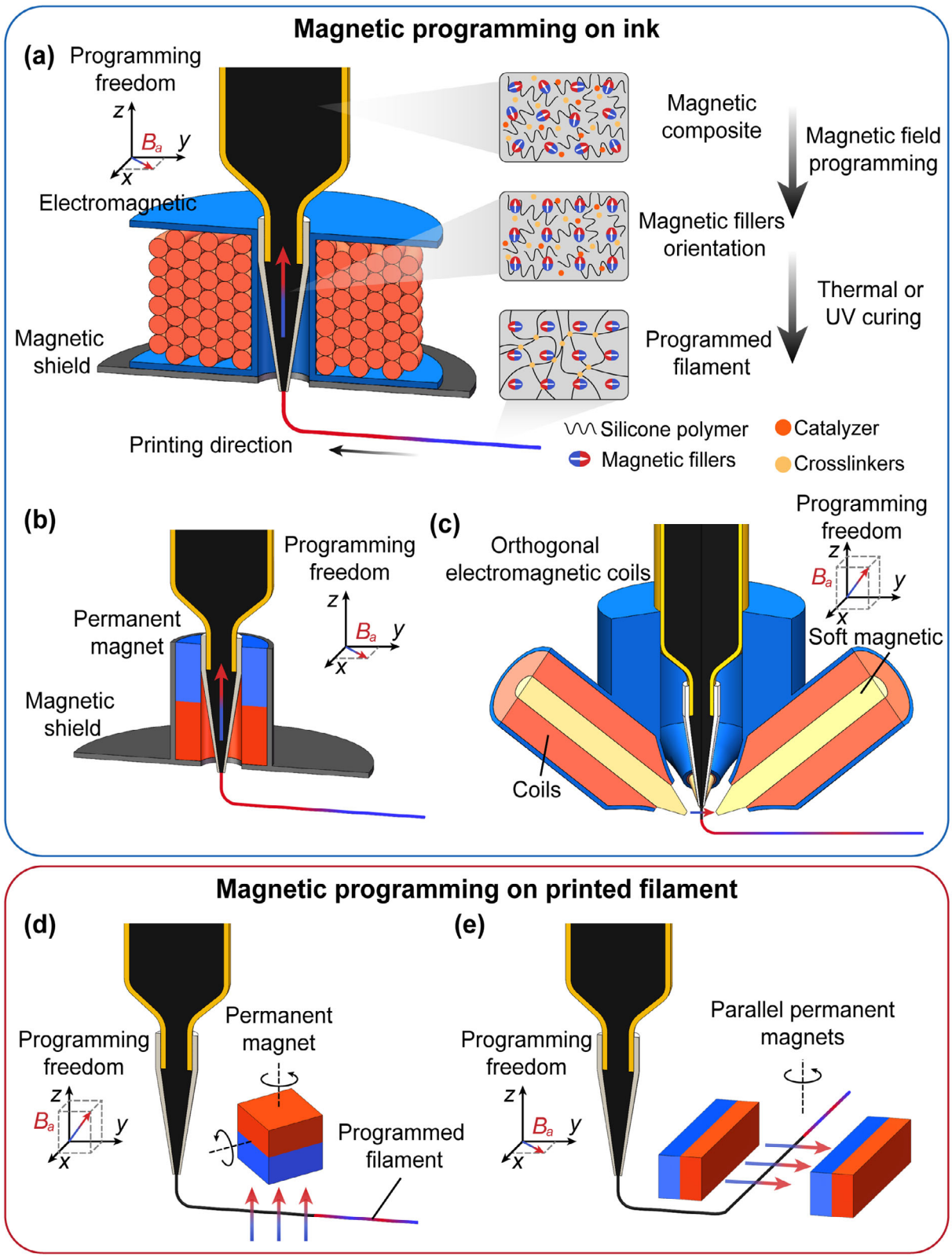

FIGURE 11 | Schematic illustration of DIW-based MF3DP systems with two magnetic programming strategies: (a–c) Magnetic programming on ink—magnetic programming is applied directly to the extruded ink during deposition, enabling in situ orientation of magnetic particles. (a) Electromagnetic coil system with magnetic shielding for localized field generation; (b) permanent magnet-based system for continuous filler alignment; (c) orthogonal electromagnetic coils combined with soft-magnetic materials for programmable multidirectional alignment. (d–e) Magnetic programming on printed filament—magnetic programming is applied after filament deposition. (d) Localized reorientation using a rotating permanent magnet; (e) alignment control using parallel permanent magnets. Colored filaments represent programmed filaments with tailored magnetization distributions or particle orientations.

Both approaches of magnetic programming on ink and on filament enable DIW-based MF3DP to manufacture various MSM 3D structures and even devices. Benefiting from the shear-thinning behavior, the viscosity of the MSM ink is significantly reduced inside the nozzle during extrusion. At the low-viscosity state, the applied magnetic field can effectively align the magnetic particles within the ink. This makes it possible to program hard-magnetic particles such as NdFeB, which are otherwise difficult to align, thereby endowing the printed structures with permanent remanent magnetization and enabling deformation or locomotion under external magnetic fields. Owing to these advantages, DIW-based MF3DP with magnetic programming on ink has been widely employed in the fabrication of magnetically active structures [32, 165], metamaterials [153, 166], and even miniature robots [82, 167].

Kim et al. developed a DIW-based MF3DP system where an electromagnet or a permanent magnet ring is integrated around the nozzle (Figure 12a) [32]. A uniaxial magnetic field (~50 mT) is applied at the nozzle to align the NdFeB microparticles (size of 5 μm, 20 vol.%) within the shear-thinned MSM ink. Once extruded, the ink retains the aligned orientation of the magnetic particles, resulting in a printed filament with a predefined magnetization direction. To realize programmable actuation behaviors, various in-plane magnetization profiles (Figure 12b) can be designed based on geometry and magnetic alignment. Under actuation magnetic fields, these patterns guide the desired deformation pathways. For example, Figure 12c presents a Miura-origami sheet and auxetic lattices that undergo folding or contraction in response to magnetic stimuli.

Expanding toward multifunctionality, Ma et al. further developed a multi-material DIW-based MF3DP system (Figure 12d), in which a permanent magnet ring is integrated around the nozzle to generate a uniaxial magnetic field (~180 mT) [166]. MSMs and magnetic shape memory polymers (M-SMPs) are co-printed to form hybrid metamaterials where MSMs and M-SMPs are precisely designed and printed (Figure 12e). Through cooperating the thermal and magnetic actuations (Figure 12f), the printed metamaterial achieves tunable physical properties such as Poisson's ratio, tunable shear, and bending deformation.

To enrich the design freedom and achieve more complex 3D magnetization profiles, Ansari et al. developed a DIW-based MF3DP system with a triaxial electromagnet (Figure 12g) [82]. Unlike the aforementioned systems, the magnetic field (~20 mT) is applied directly at the nozzle outlet rather than around the nozzle itself. This applied field aligns the NdFeB microparticles (size of 5 μm, 50 wt.%) while the ink remains in a low-viscosity state during extrusion. This configuration decouples the magnetization direction from the printing path, enabling voxel-level 3D magnetic programming. Based on this capability, Figure 12h presents a soft ribbon robot with sinusoidal magnetization that achieves wave-like locomotion under rotating magnetic fields. Furthermore, Figure 12i demonstrates a magnetic folding cube robot, which achieves sequential face closure and object encapsulation based on precisely designed magnetization orientations on each face.

One key challenge in DIW-based MF3DP with magnetic programming on filament is the difficulty of realigning magnetic particles under an applied field due to the high viscosity of the filaments after extrusion from the printing nozzle. This limitation is commonly addressed by using low-viscosity inks with highly responsive soft-magnetic particles (e.g., Fe_3O_4 nanoparticles) to enable efficient magnetic programming. Importantly, unlike hard-magnetic particles that form stable magnetization profiles after magnetic programming, soft-magnetic particles exhibit negligible remanent magnetization and therefore only develop orientation profiles after magnetic programming. Under an applied magnetic field, these particles align quickly along the field direction, imparting anisotropic mechanical, electrical, and biological properties to the printed structures. Figure 13 presents several DIW-based MF3DP systems enabled by the magnetic programming on filament approaches as well as the relevant applications.

Kokkinis et al. developed a multi-material DIW-based MF3DP system that integrates multiple nozzles and utilizes a rotating permanent magnet to generate an applied magnetic field (~40 mT) (Figure 13a) [164]. This system is capable of producing multi-material MSM structures composed of anisotropic reinforced materials (alumina platelets coated with Fe_3O_4 nanoparticles, 4.4 vol.%), rigid materials, soft materials, and support materials. As shown in Figure 13b, the magnetic programming process involves depositing the MSM ink onto the printing platform, applying a magnetic field to locally align the alumina platelets within the deposited filament, and subsequently curing the programmed regions using UV light. The final structure exhibits region-specific orientation distributions of alumina platelets (Figure 13c).

Ma et al. proposed a dual-material DIW-based MF3DP system where the applied field is provided by a rotating permanent magnet (Figure 13d) [168]. This system facilitates the fabrication of flexible sensors composed of silicon nitride (Si_3N_4)-modified liquid metal and magnetic PDMS ink (consisting of 0.15 vol.% Fe_3O_4@SiO_2 nanochains). As shown in Figure 13e, through magnetic programming, the orientation of the magnetic nanochains (NCs) in each printed layer is precisely controlled. Figure 13f presents a wear performance comparison, where the SEM images show that the multilayer NCs at a 60° rotation exhibit cleaner surfaces and reduced material migration compared with regular multilayer NCs, demonstrating the enhanced durability and performance of the printed structures with controlled magnetic particle alignment.

Additionally, the orientation of NCs can impart anisotropic biological properties. As shown in Figure 13g, Pardo et al. developed a magnetization-on-filament DIW-based MF3DP system utilizing a pair of parallel permanent magnets (14 mT) to induce applied fields [169]. Bioinks composed of gelatin-methacryloyl (GelMA) and short magnetically responsive microfibers (sMRFs, with 5% magneitc nanoparticles loaded into electrospun polycaprolactone microfibers) are printed using this system. In Figure 13h, confocal fluorescence images show the alignment of sMRFs under parallel (left) and perpendicular (right) magnetic fields, clearly demonstrating distinct orientation patterns. Finally, Figure 13i illustrates the alignment of human adipose-derived stem cells (hASCs) embedded in printed sMRFs, where magneto-mechanical stimulation during maturation activates YAP/TAZ signaling pathways, promoting cell proliferation and differentiation.

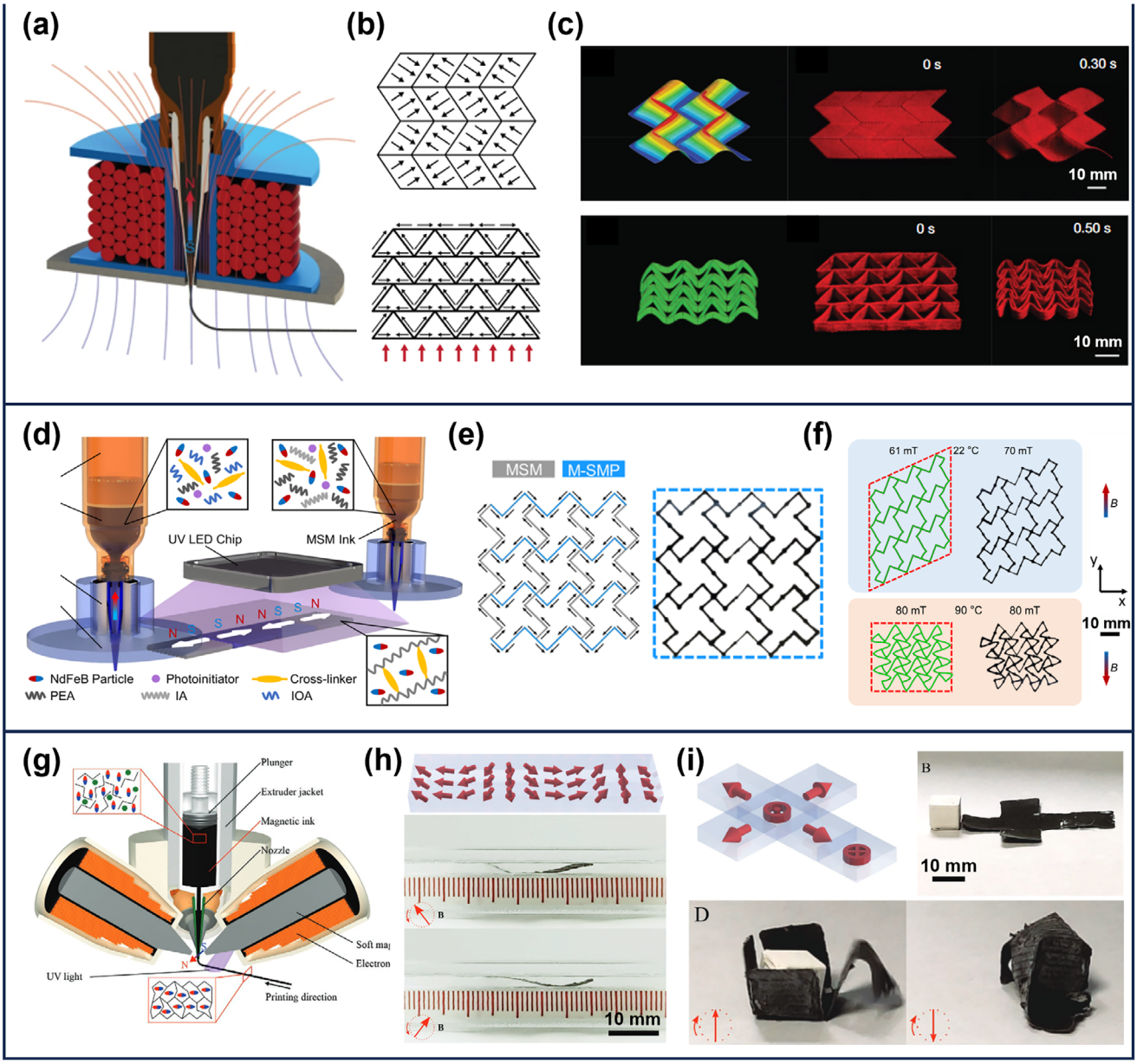

FIGURE 12 | Representative systems, magnetization profile designs, and applications of DIW-based MF3DP systems with magnetic programming on ink. (a–c) A DIW-based MF3DP system with a magnetic field generated by an electromagnet (a) enables the design of magnetization profiles (b) and the realization of complex shape transformations under magnetic actuation (c). (Reproduced with permission [32]. Copyright 2018, Springer Nature). (d–f) A multi-material DIW MF3DP system with a magnetic field generated by a permanent magnet (d) allows the fabrication of structures with designed magnetization profiles and tailored MSM/SMP domains (e), enabling printed chiral metamaterials to exhibit temperature- and magnetic-field-dependent deformation behaviors (f). (Reproduced with permission [166]. Copyright 2021, American Chemical Society). (g–i) A DIW-based MF3DP system with a magnetic field generated by a triaxial electromagnet (g) enables multidirectional magnetic programming, demonstrated by a ribbon robot showing sequential deformations (h) and a folding cube robot achieving shape morphing guided by pre-designed magnetization profiles (i). (Reproduced under the CC BY-NC 3.0 license [82]. Copyright 2023, The Authors, published by Wiley-VCH).

As summarized in Figure 14, the representative DIW-based MF3DP systems using different magnetic sources exhibit distinct trade-offs among structural configuration, programming DoFs, magnetic field strength, magnetic field uniformity, and programming area. Electromagnetic-coil-based systems are advantageous in field controllability and relatively high field uniformity, but are often constrained by limited programming area and structural complexity. Ring permanent magnets can provide stronger programming fields without overheating, but their programming freedom and field uniformity remain comparatively limited. Orthogonal coils improve programming DoFs by enabling multidirectional alignment, although they also increase system complexity and energy demand. Rotating permanent magnets are favorable for strong field strength and high programming DoFs, yet their field non-uniformity and slow mechanical adjustment reduce programming efficiency. Parallel permanent magnets are beneficial for enlarging the programming area and simplifying system design, but their weak field strength and limited

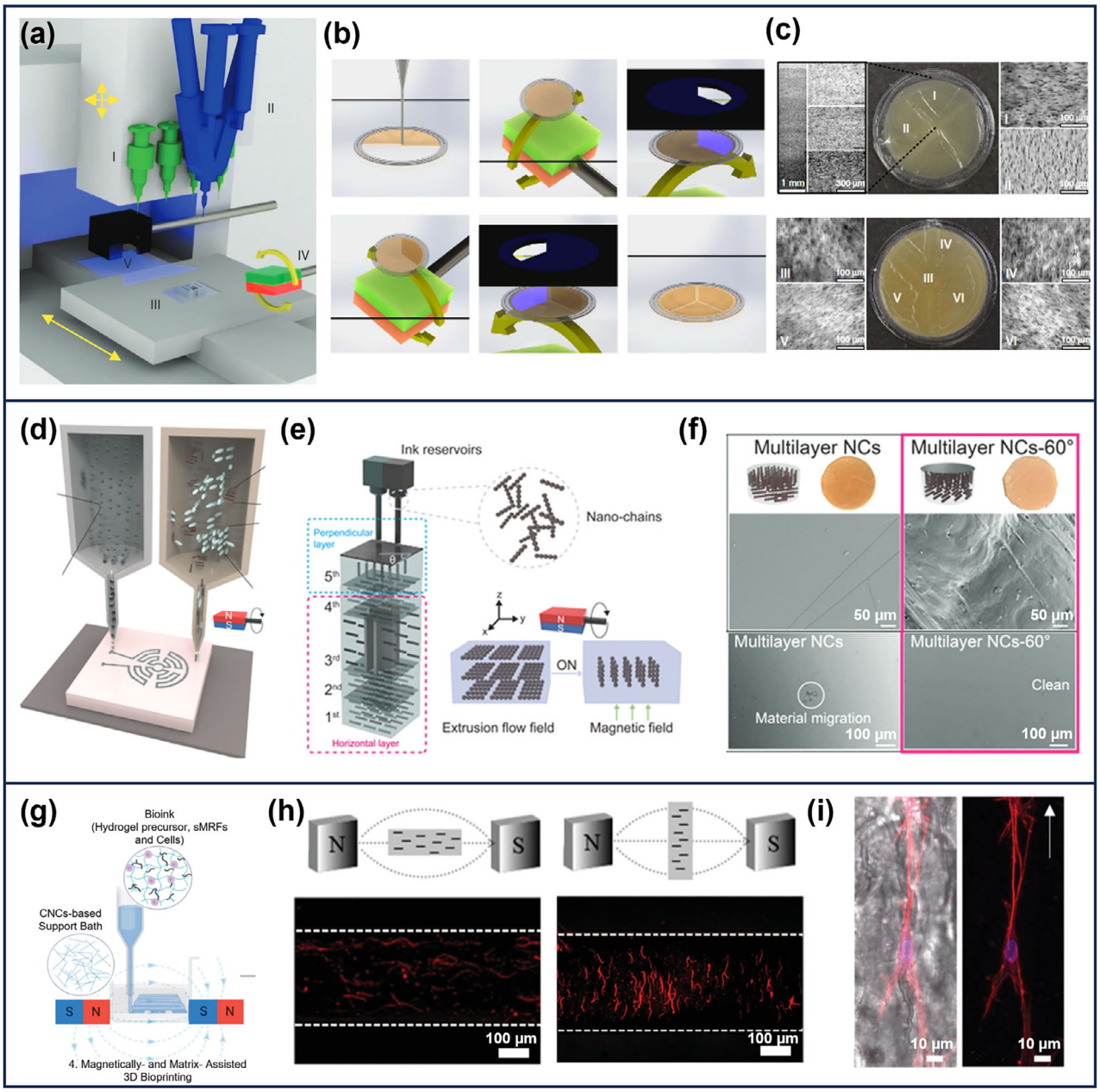

FIGURE 13 | Representative systems, orientation strategies, and applications of DIW-based MF3DP systems with magnetic programming on filament. (a–c) A multi-material DIW-based MF3DP system equipped with a rotating permanent magnet (a) enables the step-by-step fabrication of a disc structure with region-specific magnetic alignment (b), where SEM images of the top and bottom layers (c) confirm controlled platelet orientation and concentration across different regions. (Reproduced under the CC BY 4.0 license [164]. Copyright 2015, The Authors, published by Springer Nature). (d–f) A DIW-based MF3DP system utilizing a rotating permanent magnet for in situ nanochain alignment (d) allows horizontal-to-perpendicular reorientation of NCs during layer-by-layer printing (e), leading to multilayer structures with 60° rotation that exhibit cleaner surfaces and less material migration compared to unrotated samples (f). (Reproduced with permission [168]. Copyright 2024, Wiley-VCH). (g–i) A DIW-based MF3DP system employing a pair of parallel permanent magnets (g) directs the alignment of sMRFs within bioinks during printing, as verified by confocal images showing distinct alignment under parallel and perpendicular magnetic fields (h) and cytoskeletal alignment of hASCs along the printed sMRFs in anisotropic bioinks (i). (Reproduced with permission [169]. Copyright 2022, Wiley-VCH).

programming freedom confine them mainly to soft-magnetic composites. These comparisons indicate that no single DIW-based MF3DP configuration simultaneously maximizes all capabilities, and future system development should focus on balancing programming flexibility, field performance, and manufacturability according to the target application.

3.3 | Magnetic Field Assisted DLP 3D Printing

While DIW-based MF3DP relies on the extrusion of viscoelastic magnetic inks and enables localized magnetic programming during or after filament deposition, its printing resolution and geometric complexity are often limited by the rheological

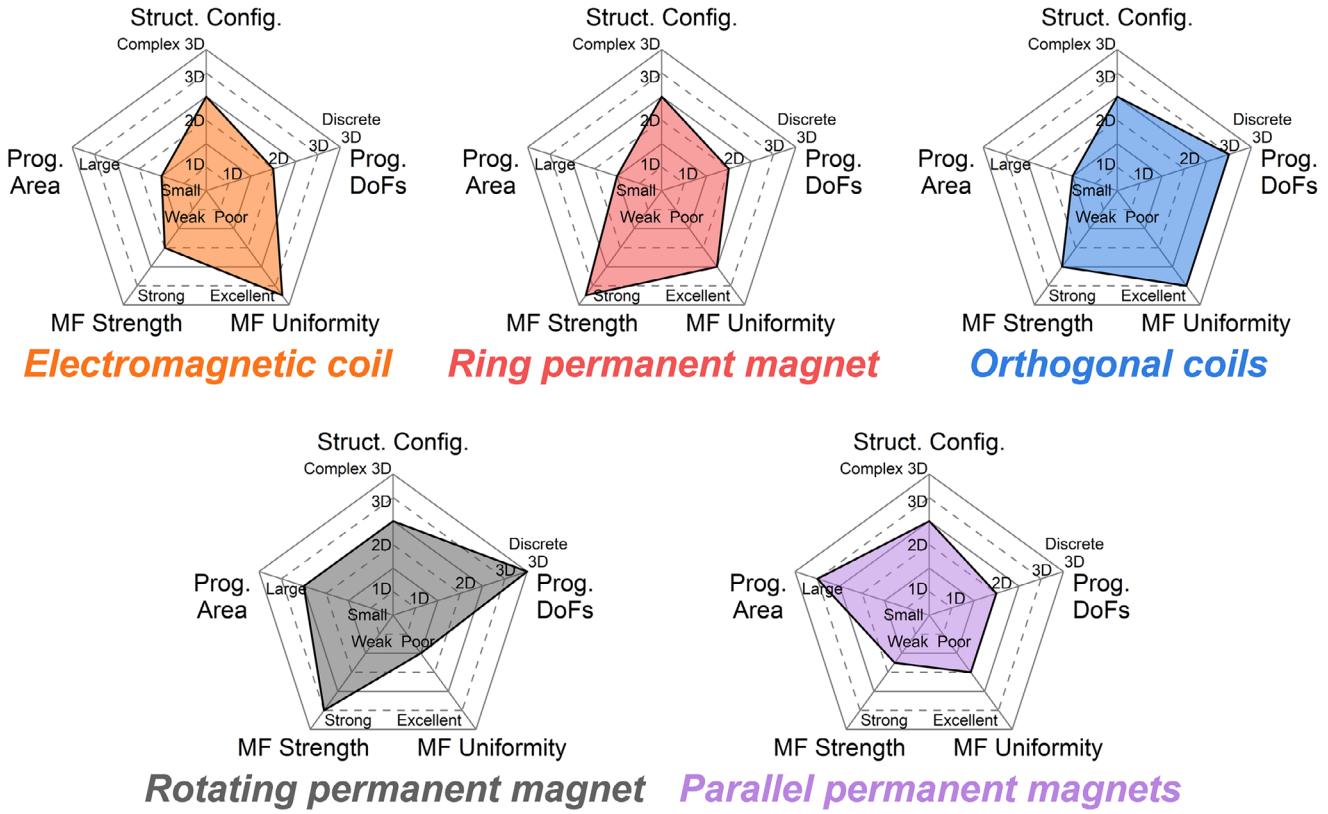

FIGURE 14 | Comparison of manufacturing capabilities and programming field performance of DIW-based MF3DP systems using different magnetic sources. The radar plots compare structural configuration (Struct. Config.; 1D to complex 3D), programming area (Prog. Area; small to large), programming degrees of freedom (Prog. DoFs; 1D to discrete 3D), magnetic field strength (MF Strength; weak to strong), and magnetic field uniformity (MF Uniformity; poor to excellent).

behavior of the ink and the nozzle size. In contrast, DLP-based MF3DP employs photocurable resins and voxel-level projection curing, which significantly enhances printing precision and scalability. By integrating external magnetic fields into the DLP process, magnetic particle alignment can be achieved throughout the entire resin vat prior to photopolymerization, enabling uniform magnetic programming and the fabrication of complex magnetically functional structures. Accordingly, understanding the characteristics of magnetic field sources and their influence on particle orientation is essential for designing and optimizing DLP-based MF3DP systems.

In DLP-based MF3DP, magnetic particles are uniformly dispersed in the photocurable resin within the vat, and the applied magnetic field acts on the entire resin volume to orient the particles through magnetic torque (or a combination of torque and force). Since the efficiency of this particle orientation is determined by the characteristics of the applied field, the choice of magnetic field source becomes critical. Different sources vary in terms of field strength, uniformity, programming freedom, and effective programming area, and these differences directly define the manufacturing capabilities of DLP-based MF3DP systems. They affect not only the efficiency and accuracy of magnetic programming but also the uniformity of particle concentration in the printed MSM structures, the achievable programming freedom, the effective build area, and the structural complexity that can be fabricated. As illustrated in Figure 15, DLP-based MF3DP systems can therefore be divided into three categories according to the type of field source: (a) magnetic programming via electromagnetic coils [16, 17, 170, 171], (b–c) magnetic programming via permanent magnets [33, 126, 163, 172–176], and (d) magnetic programming via hybrid magnetic sources that combine Halbach arrays with electromagnetic coils [80].

As shown in Figure 15a, the earliest DLP-based MF3DP systems were developed using large orthogonal electromagnetic coils (such as Helmholtz coils) positioned directly around the resin vat. By adjusting the current magnitude and direction in each axis coil, a 3D magnetic field with tunable orientation and intensity can be applied. During printing, the applied magnetic field is first aligned with the desired programming direction and maintained for a period, allowing the initially randomly oriented magnetic particles in the photocurable resin to gradually reorient. Once particle alignment is achieved, the DLP projector projects UV light to cure the resin, permanently locking the orientation of the particles through the polymer crosslinked network. This process is repeated to fabricate MSM domains with different programming directions within the same layer, and layer-by-layer stacking eventually yields the complete MSM structure. Although electromagnetic coils provide full 3D programming freedom, they are limited in delivering high field strengths or sustaining long printing durations, as high power or prolonged operation leads to overheating.

Similar to DIW-based MF3DP systems, permanent magnets can be used to overcome the overheating issue. As illustrated in

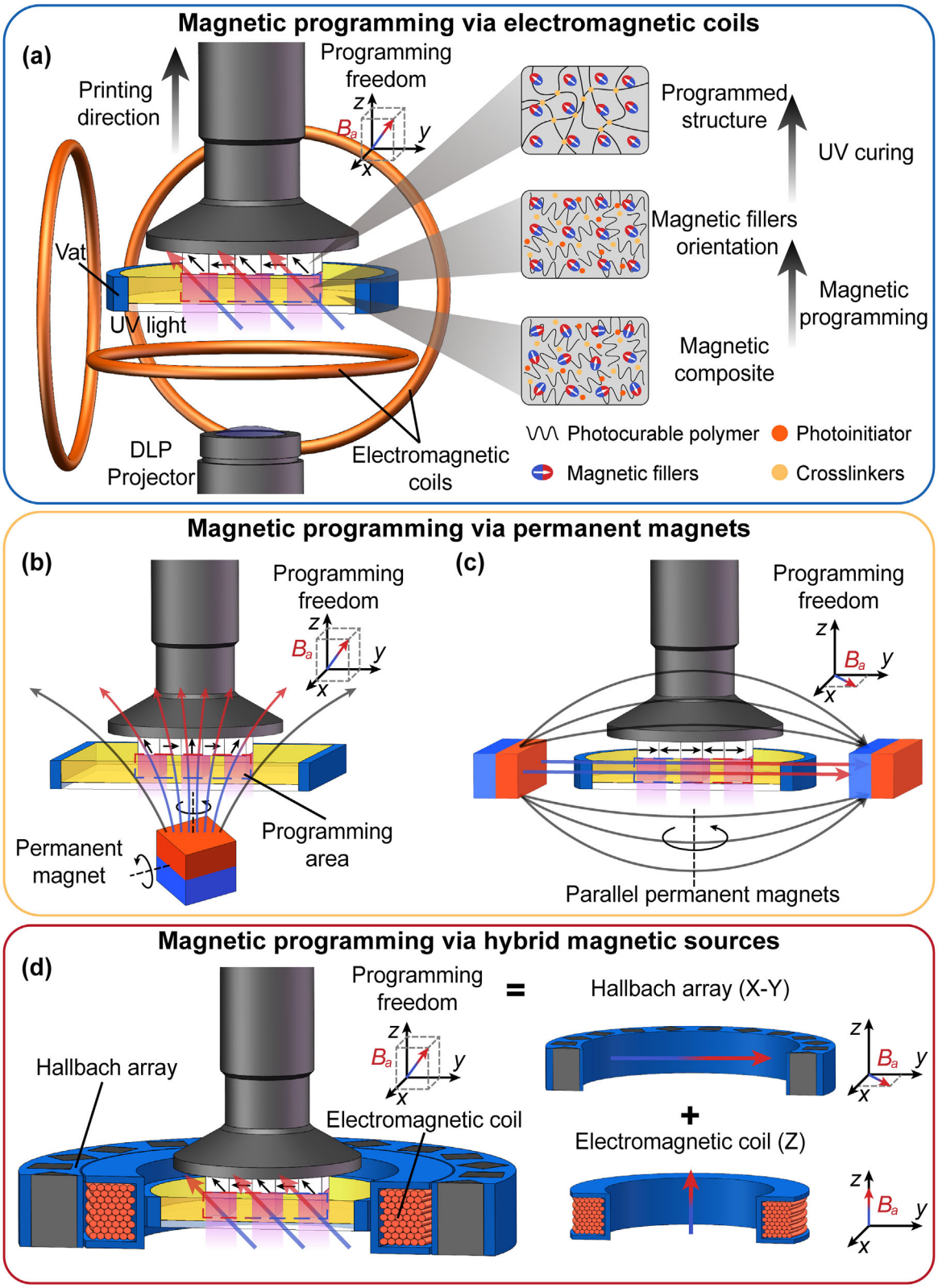

FIGURE 15 | Schematic illustration of DLP-based MF3DP systems categorized by magnetic field source. (a) Magnetic programming via electromagnetic coils–orthogonal coils or Helmholtz coils provides a uniform magnetic field with a low gradient, allowing full 3D programming. (b, c) Magnetic programming via permanent magnets, (b) a single rotating permanent magnet generates a non-uniform field with a high gradient, enabling 3D programming; (c) parallel rotating permanent magnets produce a relatively uniform field with a high gradient and a large area, offering only 2D programming. (d) Hybrid magnetic source, which integrates a Halbach array for strong, uniform in-plane fields (X–Y) with an electromagnetic coil for out-of-plane fields (Z), achieving high uniformity and full 3D programming capability.

Figure 15b, in a DLP-based MF3DP system with magnetic programming via a rotating permanent magnet, a cubic or cylindrical magnet is placed beneath the resin vat and rotated in space, thereby providing full 3D magnetic programming freedom. Benefiting from the magnetic field distribution of a cubic or cylindrical permanent magnet, the strength of the applied field can be easily increased by simply reducing the distance between the magnet and the vat bottom, thereby greatly improving programming efficiency. However, decreasing this distance simultaneously increases the gradient of the applied field, which induces particle aggregation and sedimentation. Moreover, the gradient field exerts both magnetic torque and force on previously printed MSM structures with programmed magnetization, often leading to deformation of printed MSM structures. As a result, this type of DLP-based MF3DP system is not well-suited for fabricating complex 3D MSM structures.

As shown in Figure 15c, placing a pair of parallel permanent magnets around the resin vat is an effective way to reduce the applied field gradient, provided that the magnets are positioned sufficiently far apart. Compared with a single rotating permanent magnet, this type of DLP-based MF3DP system generates a more uniform magnetic field. However, the achievable field strength remains relatively low (typically 10–20 mT), which means it can only be used to program particles with strong magnetic responsiveness (such as soft-magnetic particles). In addition, this type of DLP-based MF3DP system only provides 2D magnetic programming freedom, thereby limiting the complexity of MSM structures that can be fabricated.

Unlike the aforementioned magnetic sources, hybrid sources combine their respective advantages while avoiding their shortcomings. As shown in Figure 15d, a Halbach array provides 2D magnetic programming freedom in the X–Y plane, while an electromagnetic coil supplies 1D magnetic programming freedom in the Z direction, together achieving 3D magnetic programming capability. Benefiting from the high field strength and high uniformity provided by both the Halbach array and the electromagnetic coil, the combined magnetic field reaches a high intensity (~80 mT) with excellent uniformity (gradient < 5 mT), and it can operate continuously without overheating. This enables this type of DLP-based MF3DP system to fabricate complex MSM structures with full 3D magnetic programming freedom. Nevertheless, the applied field may still cause deformation in previously printed MSM structures, requiring a large number of support structures to ensure stability. As a result, additional post-processing steps are needed to remove the supports, which increases the overall complexity of the fabrication process.

The representative DLP-based MF3DP systems differ mainly in orientation speed, programming area, field strength, field gradient, sustainable working time, and energy consumption, which in turn determine their programming capability and manufacturing performance. Their key characteristics are summarized in Table 2.

Electromagnetic coils are advantageous in DLP-based MF3DP because they enable real-time control of field direction and magnitude, thereby offering the highest magnetic programming flexibility among the available field sources. The programming field direction and magnitude can be changed in real time by

TABLE 2 | Key performance comparison of different magnetic sources used in DLP-based MF3DP systems.

Magnetic field source	Orientation speed	Programming area	Field strength	Field gradient	Sustainable working time	Energy consumption
Electromagnetic coils	Fast, real-time electrical switching	Adjustable by coil size, but larger coils reduce intensity	Moderate, limited by power	Low (Helmholtz configuration ensures uniformity)	Limited, prone to overheating	High
Single rotating permanent magnet	Slow, depends on mechanical rotation	Localized, rapidly decays with distance	High, suitable for hard-magnetic particles	High, non-uniform, strong gradients	Long, stable without heating issues	Very low
Parallel rotating permanent magnets	Relatively fast, single-axis rotation	Larger central region between magnets	Low, decreases with increased spacing	Reduced compared with a single magnet, more uniform	Long, stable operation	Very low
Hybrid magnetic sources (Halbach + coil)	Fast, Halbach rotation + coil adjustment	Large, uniform coverage	High, with low gradients	Low, uniform field distribution	Long, stable with standard cooling	Moderate

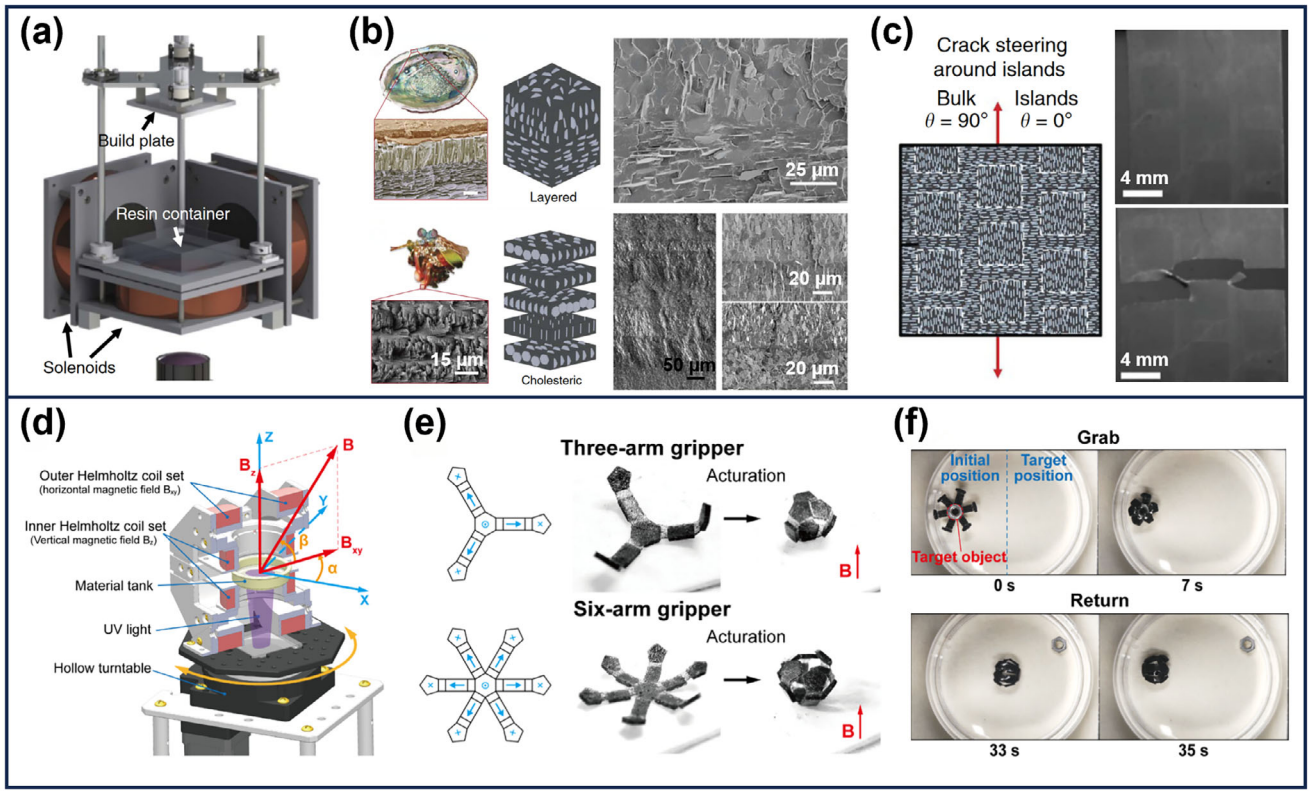

FIGURE 16 | Representative systems, programmed MSM structures, and applications of DLP-based MF3DP systems incorporating magnetic programming via electromagnetic coils. (a) A system integrated with externally orthogonal electromagnetic coils. (b) Bioinspired layered and helicoidal architectures with ordered particle alignment. (c) Island–matrix design with locally contrasting orientations. (Reproduced under the CC BY 4.0 license [170]. Copyright 2015, The Authors, published by Springer Nature). (d) A system integrated with nested Helmholtz coils and a rotary stage for uniform 3D fields. (e) Three- and six-arm flexible grippers. (f) Six-arm gripper capturing and returning target objects under magnetic actuation. (Reproduced with permission [171]. Copyright 2024, Elsevier).

adjusting the current in each axis coil, which allows rapid field reorientation during printing. The programming area can be enlarged by increasing the coil size, but this usually lowers the field strength because of power limits. When the coils are arranged in a Helmholtz configuration, they produce uniform fields with low gradients, which help align magnetic particles accurately and reduce sedimentation. However, electromagnetic coil systems consume large amounts of energy and heat up quickly. As a result, they cannot operate stably for long periods, which limits the fabrication of complex 3D MSM structures. At the same time, cooling equipment becomes necessary, adding further complexity and cost to the MF3DP system.

As shown in Figure 16a, Martin et al. introduced a DLP-based MF3DP system that integrates externally orthogonal electromagnetic coils [170]. An acrylate-based photocurable resin was used as the matrix, into which alumina platelets were incorporated after magnetic particles (Fe_3O_4) labeling, with a typical loading of ~15 vol.%. During printing, the particles were aligned under external magnetic fields and subsequently fixed in place by UV curing. As shown in Figure 16b, they successfully reproduced natural bioinspired reinforcement structures, such as the layered structure of the abalone shell and the helicoidal structure of the mantis shrimp's dactyl club, both showing highly ordered particle alignment within the matrix. As illustrated in Figure 16c, they further designed "island–matrix" structures with locally contrasting orientations, which redirected crack propagation through a mechanism of crack steering. By forcing cracks to deflect along programmed pathways, the printed composites exhibited enhanced fracture resistance.

As shown in Figure 16d, Sun et al. developed a DLP-based MF3DP system that is integrated with nested Helmholtz coils and a hollow rotary stage [171]. A flexible photocurable resin (RESIONE F39T) was used as the matrix, into which oleic-acid-modified NdFeB microparticles (size of 5 μm, 10 wt.%) were dispersed. The particles were pre-magnetized under a strong external field (4 T) prior to printing, ensuring maximum remanent magnetization. As illustrated in Figure 16e, they fabricated multi-arm flexible grippers in which programmed magnetization profiles enabled rapid and controlled deformation. As shown in Figure 16f, performance tests further confirmed that the six-arm gripper could enclose, transport, and return target objects within seconds, highlighting both stable actuation and practical functionality.

Single rotating permanent magnets are attractive in DLP-based MF3DP because they can generate strong and stable magnetic fields without electrical input, making them suitable for programming hard-magnetic particles. Because no current is required, they avoid high energy consumption and overheating, allowing continuous operation for long periods. The drawback is that the programming field reorientation depends on mechanical

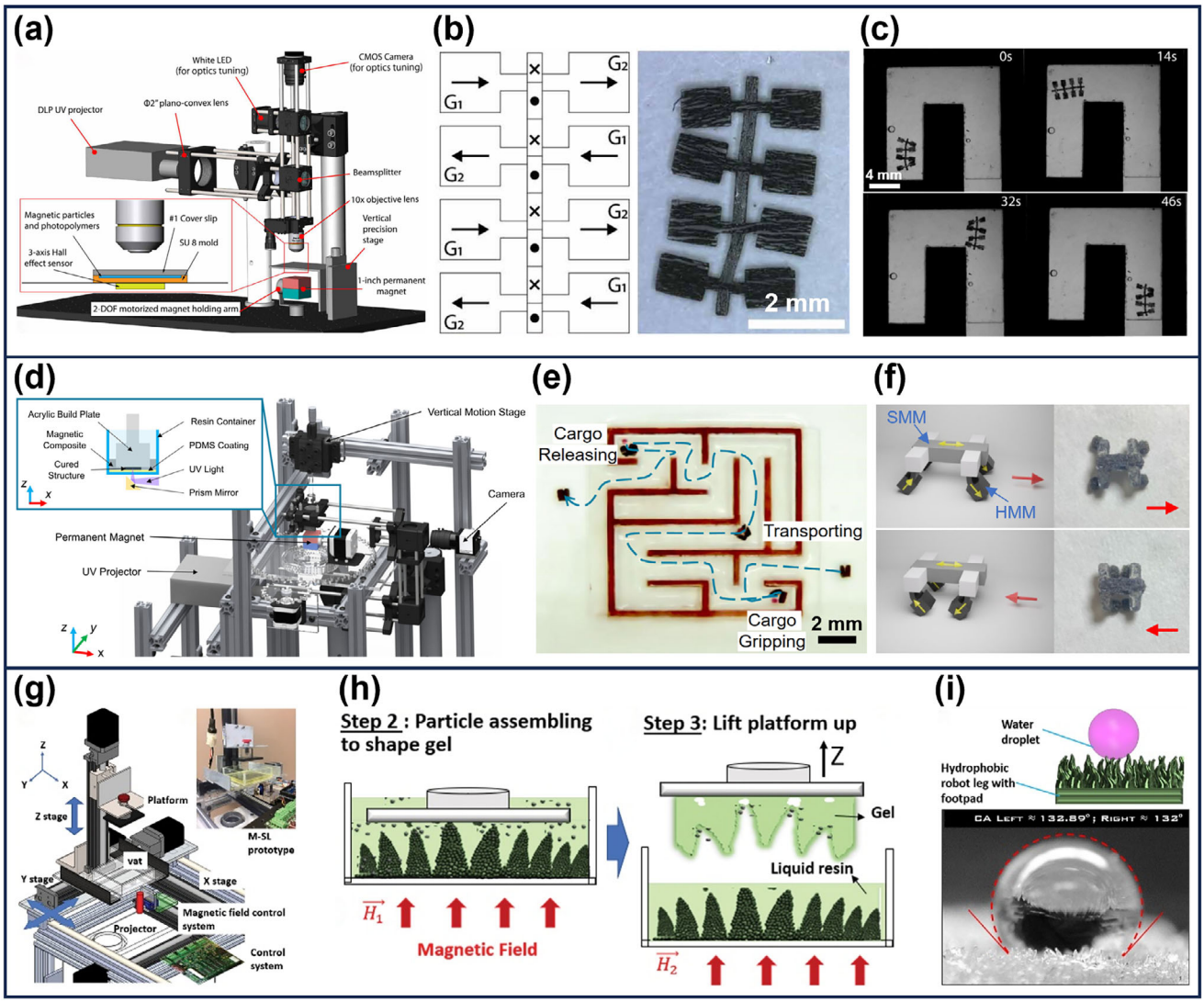

FIGURE 17 | Representative systems, programmed MSM structures, and applications of DLP-based MF3DP systems incorporating magnetic programming via a single rotating permanent magnet. (a) A system integrated with a two-DoFs permanent magnet. (b) Magnetization profile and image of a paddle-crawling microrobot. (c) Top-view images showing the locomotion of the robot in a microchannel filled with silicone oil. (Reproduced with permission [33]. Copyright 2019, American Association for the Advancement of Science). (d) A multilayer and multimaterial system integrated with a two-DoFs permanent magnet. (e) A capsule-like robot performing gripping, transporting, and releasing tasks. (f) A four-legged robot combining HMM and SMM materials for stable bidirectional walking. (Reproduced under the CC BY 3.0 license [172]. Copyright 2024, The Authors, published by Wiley-VCH). (g) A system integrated with a permanent magnet. (h) Magnetic field-guided assembly of ferrite nanoparticles into multi-scale spike arrays. (i) Spiked footpads exhibiting hydrophobicity. (Reproduced with permission [173]. Copyright 2022, Mary Ann Liebert).

rotation, so the adjustment speed is relatively slow. The effective programming area is limited to regions close to the magnet, since the field strength decreases rapidly with distance. At the same time, the field shows steep gradients, which reduce uniformity, promote particle sedimentation, and may apply extra forces and torques to printed MSM structures. These effects can cause deformation or even printing failure, making it difficult to fabricate complex 3D MSM structures despite the advantage of high field strength and long operating time.

As shown in Figure 17a, Xu et al. introduced a DLP-based MF3DP system that integrates a two-DoFs permanent magnet [33]. The printing material consisted of a UV-curable elastomeric resin matrix loaded with pre-magnetized NdFeB microparticles (size of ~5 μm, pre-magnetized in a 1.1 T uniform magnetic field) at a 1:1 mass ratio, providing both strong magnetic response and reliable printability. As illustrated in Figure 17b, they fabricated an eight-legged paddle-crawling microrobot in which the legs carried alternating magnetization profiles. As illustrated in Figure 17c, experiments further confirmed its ability to move stably in liquid environments and navigate confined microchannels.

As shown in Figure 17d, Li et al. developed a multilayer and multimaterial DLP-based MF3DP system that integrates a two-DoFs permanent magnet [172]. The materials included hard-magnetic materials (HMM) made of flexible UV resin (Elastic 50A) loaded with NdFeB microparticles (size of ~5 μm, pre-magnetized in a 2.4 T uniform magnetic field) and soft-magnetic materials (SMM)

prepared from a rigid UV resin (Clear V4) with iron particles. This multimaterial strategy endowed the printed robots with distinct mechanical and magnetic properties. As illustrated in Figure 17e, they fabricated capsule-like robots capable of gripping, transporting, and releasing cargo along complex pathways. In addition, as illustrated in Figure 17f, a four-legged walking robot integrated HMM and SMM regions, enabling stable bidirectional locomotion under magnetic actuation.

As shown in Figure 17g, Joyee et al. introduced a DLP-based MF3DP system that integrates a permanent magnet to induce particle assembly during printing, enabling direct fabrication of soft robot footpads with multi-scale spike arrays [173]. The printing material consisted of a flexible UV resin (Spot E elastic) loaded with 60–80 wt.% ferrite nanoparticles (size of ~10 nm), providing both strong magnetic responsiveness and the ability to align under an applied programming field. As illustrated in Figure 17h, during printing, the particles assembled into conical arrays under the applied field and were locked in place by sequential curing. As illustrated in Figure 17i, the resulting bioinspired spiked footpads drastically altered the surface wettability, switching from hydrophilic to hydrophobic with a measured contact angle of ~132°.

Compared with a single rotating permanent magnet, parallel permanent magnets provide a larger programming region (i.e., the central region) with reduced field gradients, which is beneficial for improving field uniformity and alignment stability. Increasing the spacing between the magnets can further reduce gradients, but also decreases the field strength. The programming field reorientation speed is relatively fast, since only single-axis rotation is needed. However, the programming fields are much weaker than those of single magnets, which means that the system can only program soft-magnetic particles. Another drawback is that parallel magnets only provide 2D programming freedom, which greatly restricts the programming design flexibility of MSM structures. In addition, the relatively low field strength limits the choice of magnetic particles and makes this configuration suitable mainly for soft-magnetic particles.

As shown in Figure 18a, Li et al. developed a DLP-based MF3DP system that integrates parallel permanent magnets for aligning nanoparticle bundles within a polymer matrix [174]. The composite material consisted of a photocurable resin (Eglass) loaded with carbonyl iron particles (size of 3–5 μm, mass ratios of 5–25 wt.%) and iron oxide nanoparticles (size of < 50 nm, mass ratios of 0.25–3.25 wt.%), which assembled into vertically oriented bundles during curing. As illustrated in Figure 18b, inspired by the hierarchical architecture of limpet teeth, this design enhanced the strength and buckling resistance of microneedles. As illustrated in Figure 18c, experiments showed that even with diameters as small as 50 μm, the printed microneedles retained sharp, intact tips capable of penetrating PDMS artificial skin without fracture.

As shown in Figure 18d, Wu et al. developed a DLP-based MF3DP system that integrates parallel rotating permanent magnets [175]. The resin formulation consisted of 4-hydroxybutyl acrylate (4-HBA), heavily loaded with carbonyl iron powder (CIP, size of ~7 μm, mass ratios up to 45 wt.%) and stabilized by fumed silica to avoid sedimentation. Under the applied field, the CIP particles assembled into chain-like structures that were fixed within the polymer. As illustrated in Figure 18e, they fabricated an arrow-shaped sample with four different chain alignment configurations (90°, 45°, 0°, and −45°). As illustrated in Figure 18f, when floated on water and exposed to horizontal magnetic fields, the arrows rotated according to their programmed alignment, resulting in four distinct stable orientations.

With the same DLP-based MF3DP system setup as shown in Figure 18g, Wu et al. further designed TPMS magnetic self-powered sensors [126]. The composites used 4-HBA and acrylate-based polyurethane diacrylate (AUD) as the matrix, with 20 wt.% carbonyl iron powder (CIP, size of ~2.5 μm) serving as the magnetic filler. Under the programming field, CIP particles aligned uniformly, enabling stronger magnetic responsiveness in the aligned direction. As illustrated in Figure 18h, this effect was validated by comparing enhanced and non-enhanced TPMS samples in an actuation test, where enhanced samples responded more quickly under an external magnetic field. As illustrated in Figure 18i, an S-type TPMS lattice was integrated into a self-powered electromagnetic sensing setup, where compressive loading induced coil voltage outputs, confirming stable electromechanical conversion.

Pushing the DLP-based MF3DP system toward multifunctionality, as shown in Figure 18j, Wu et al. developed a multimaterial DLP-based MF3DP system that integrates parallel rotating permanent magnets [176]. The resin used a flexible acrylate-based SMP matrix (2-hydroxyethyl methacrylate, HEMA/AUD/IBOA) loaded with Fe_3O_4 microparticles (size of ~1 μm, up to 20 wt.%) and a small amount of multi-walled carbon nanotubes (MWCNTs, ≤0.5 wt.%). Fe_3O_4 imparted magnetic responsiveness and inductive heating capability, while CNTs provided sufficient electrical conductivity for Joule heating. As illustrated in Figure 18k, they printed complex 3D architectures using this system. As illustrated in Figure 18l, a flower-like actuator with outer and inner petals of distinct compositions produced sequential blooming under electrical stimulation.

Hybrid magnetic sources combine a Halbach array in the X–Y plane with an electromagnetic coil along the *Z*-axis, integrating the advantages of both permanent magnets and electromagnetic coils. This setup provides high field strength, good field uniformity, low gradients, and a large programming area, making it the most balanced DLP-based MF3DP configuration currently reported. Programming field reorientation can be adjusted quickly: the Halbach array is rotated mechanically to reorient the in-plane field, and the *Z*-axis component is tuned electrically. A small single-axis electromagnetic coil is used only to generate the *Z*-axis field, and heating can be managed effectively with standard cooling, allowing stable long-term operation at a moderate energy cost. With the combination of strong fields, low gradients, large programming areas, and reliable working time, hybrid magnetic source systems are particularly well suited for manufacturing complex 3D MSM structures. The main drawback is the higher system complexity and cost, but they currently represent the most balanced solution for advanced DLP-based MF3DP systems.

As shown in Figure 19a, Meng et al. developed a DLP-based MF3DP system that combines a Halbach permanent magnet

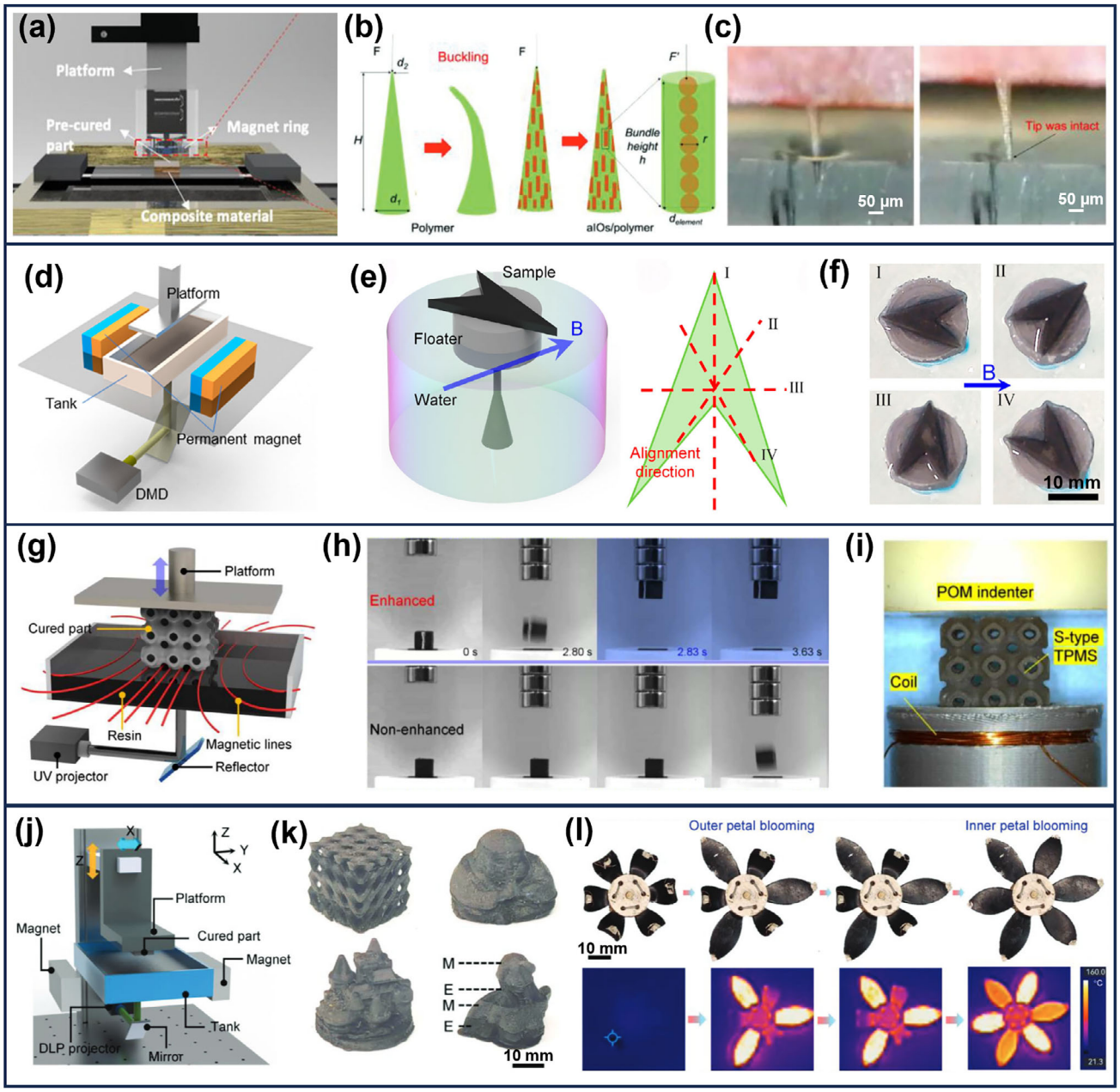

FIGURE 18 | Representative systems, programmed MSM structures, and applications of DLP-based MF3DP systems incorporating magnetic programming via parallel rotating permanent magnets. (a) A system integrated with parallel permanent magnets. (b) Oriented nanoparticle bundles reinforcing microneedles against buckling. (c) Sharp, intact microneedle tips (50 μm) successfully penetrated PDMS skin models. (Reproduced with permission [174]. Copyright 2021, Wiley-VCH). (d) A system integrated with parallel permanent magnets. (e) An arrow-shaped sample with four different chain alignment configurations. (f) Final alignment states of configurations I–IV under the same actuation field directions. (Reproduced under the CC BY 4.0 license [175]. Copyright 2023, The Authors, published by Taylor & Francis). (g) A system integrated with parallel permanent magnets. (h) The movement of the enhanced and non-enhanced cubic sample when the magnet is approaching. (i) An S-type TPMS-based sensor. (Reproduced under the CC BY 4.0 license [126]. Copyright 2024, The Authors, published by Taylor & Francis). (j) A multimaterial system integrated with parallel permanent magnets. (k) Printed multimaterial structures combining electric and magnetic SMPs. (l) Flower-like actuator showing sequential blooming under electrical heating. (Reproduced with permission [176]. Copyright 2024, Wiley-VCH).

array with an electromagnetic coil to generate strong, highly uniform, and 3D magnetic programming fields [80]. The photocurable resin was based on a silicone elastomer, into which ~20 wt.% NdFeB microparticles (size of 1–2 μm) were dispersed. To assess printing fidelity and magnetization control, the authors quantified the angular deviation of particle alignment under different printing conditions. As illustrated in Figure 19b, results showed that the hybrid magnetic source system achieved high alignment accuracy (directional errors lower than 1.3°) and high uniformity (field strength inhomogeneity lower than 5%), confirming the robustness of the programming field control for large-area fabrication.

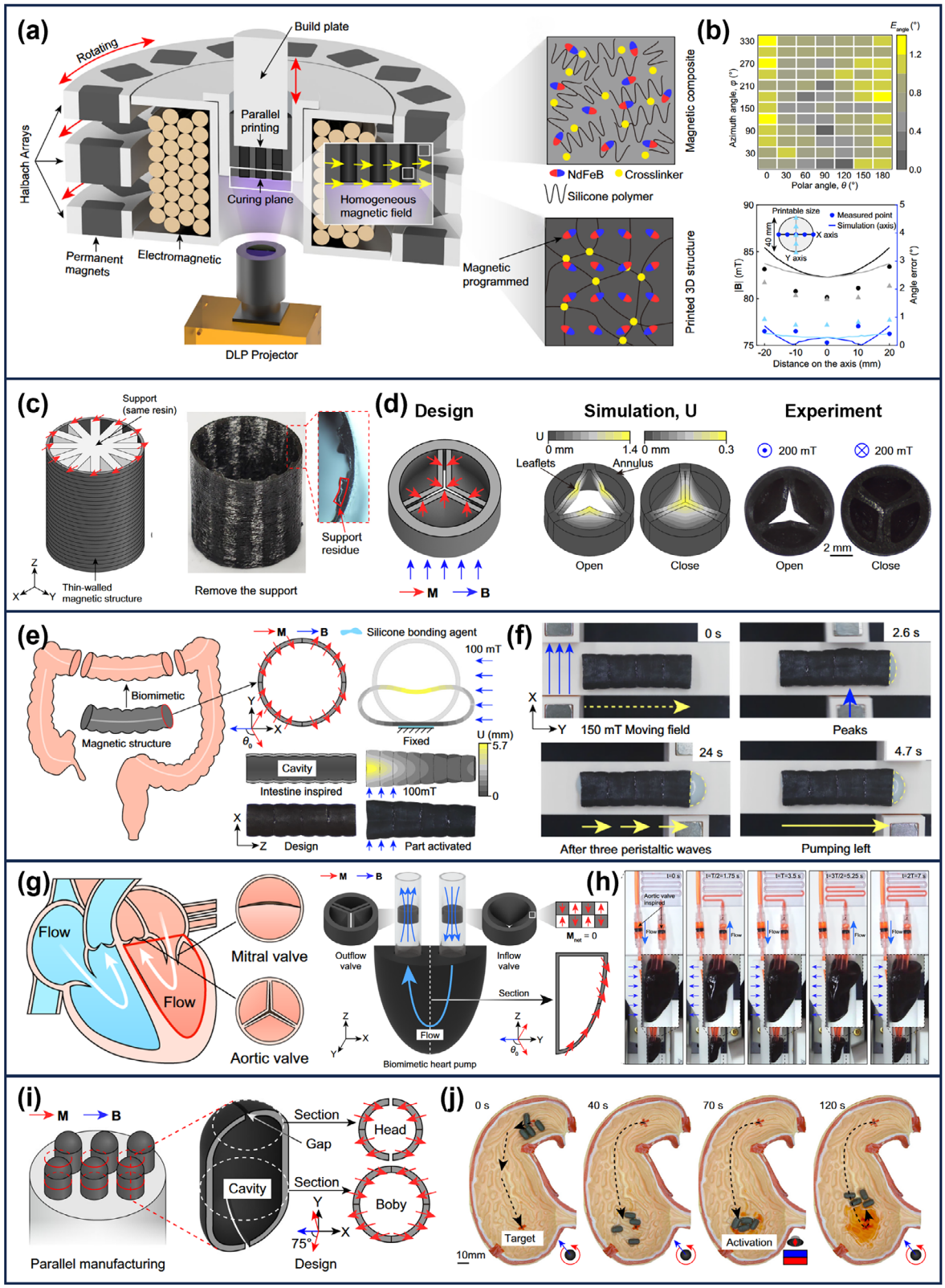

FIGURE 19 | System setup and applications of a DLP-based MF3DP system incorporating magnetic programming via hybrid magnetic sources. (a) System setup. (b) Uniformity and accuracy of the magnetic field strength and direction on the printing plane. (c) Thin-walled tubular structures with removable supports. (d) One-way valves inspired by aortic valves. (e) Intestinal-inspired tubular actuator design. (f) Peristaltic pumping under moving magnetic fields. (g) Biomimetic heart pump with magnetized valves. (h) Sequential images show fluid flow through the pump at different time points. (i) Capsule-like robot with head–body magnetization profiles. (j) Capsule actuation showing rolling and payload release. (Reproduced under the CC BY 4.0 license [80]. Copyright 2024, The Authors, published by Springer Nature).

As illustrated in Figure 19c, free-standing thin-walled tubular structures were printed with sacrificial supports, which could be removed after curing to yield cavity-rich architectures with high porosity and structural integrity. These thin-walled geometries were further exploited to design several biomimetic machines. As illustrated in Figure 19d, a trileaflet magnetic valve, mimicking cardiac valves, was fabricated and tested. Both simulations and experiments demonstrated that the valve opened under forward actuation magnetic fields but closed rapidly under reverse fields, thereby ensuring unidirectional liquid transport. As illustrated in Figure 19e, inspired by intestinal peristalsis, the team also designed a soft tubular actuator with circumferential magnetic domains programmed along its wall. When actuated by a moving magnetic field of ∼150 mT, sequential contraction waves propagated along the tube, transporting viscous liquid unidirectionally. As illustrated in Figure 19f, experimental recordings confirmed effective peristaltic pumping, validating the concept as a biomimetic peristaltic machine.

As illustrated in Figure 19g, the DLP-based MF3DP system was next applied to create a biomimetic heart pump consisting of a conical thin-walled cavity with oppositely magnetized inflow and outflow valves. Subjected to alternating magnetic fields, the cavity exhibited cyclic expansion and contraction, resembling ventricular systole and diastole. As illustrated in Figure 19h, the magnetic pump achieved cyclic filling and contraction, driving unidirectional fluid flow that mimics a biological heartbeat.

As illustrated in Figure 19i, a capsule-like soft robot was fabricated. The capsule was divided into head and body sections with distinct programmed magnetization profiles. Under a rotating magnetic field, the robot rolled controllably across surfaces, and under a strong localized field, the head section opened to release its internal payload. Figure 19j illustrates the robot's ability to navigate, activate, and perform targeted liquid delivery or sampling, highlighting its potential in biomedical applications such as drug delivery and minimally invasive diagnostics.

Overall, this set of demonstrations shows how a hybrid magnetic sources DLP-based MF3DP system enables the fabrication of thin-walled, cavity-rich magnetic soft machines with programmable anisotropy, providing new opportunities for mimicking essential biological functions, including flow control, peristaltic pumping, cardiac circulation, and capsule-based transport.

In summary, the performance of DLP-based MF3DP is fundamentally determined by the characteristics of the programming magnetic source. As shown in Figure 20, electromagnetic coils offer the highest programming freedom and excellent field uniformity, but their relatively weak field strength and high energy consumption restrict long-term stability. Rotating permanent magnets provide strong fields and full 3D programming freedom, yet their limited programming area, poor uniformity, and slow mechanical adjustment reduce efficiency in fabricating complex structures. Parallel permanent magnets improve field uniformity and enlarge the programming area, but their weak field strength and restriction to 2D programming freedom confine them to soft-magnetic systems. Hybrid magnetic sources combine relatively high field strength, high field uniformity, large programming area, and high programming DoFs, and therefore currently represent the most balanced solution for DLP-based MF3DP. Taken together, these comparisons indicate that the manufacturing capabilities of DLP-based MF3DP systems are governed by the balance among field strength, field uniformity, programming freedom, and effective programming area. Future development should therefore focus on improving this balance to better support the fabrication of complex MSM structures for diverse application scenarios.

4 | Perspective

In the preceding sections, we have provided a comprehensive overview of recent advances in 3D printing of MSMs, covering material foundations (magnetic particles, matrices, composites, and their responsive behaviors), traditional manufacturing approaches, and 3D printing of MSMs followed by post magnetic programming, while placing particular emphasis on MF3DP. For MF3DP, we have discussed in depth the performance of programming magnetic fields, strategies for magnetic field integration, the overall manufacturing capabilities of different systems, and representative structures and applications for each system. Numerous 3D printing systems have been used to fabricate various 3D MSM structures for application in biomedical devices, flexible sensors, and miniature robots. However, the broader development of 3D-printed MSM structures and devices depends not only on advances in manufacturing capability itself, but also on progress in material integration, computationally guided design, and reconfigurable magnetic functionality. As summarized in Figure 21, three aspects appear to be particularly important for the future development of 3D printing of MSMs: multi-material integration, computationally guided design that combines modeling, inverse design, and ML-assisted optimization, and reconfigurable magnetization for dynamic and multifunctional MSM structures.

4.1 | Multi-Material Integration

Multi-material integration encompasses combinations such as soft/hard materials, active/passive materials, and magnetic/non-magnetic materials. This capability is crucial for creating multifunctional devices, yet two key challenges persist. First, low interfacial bonding strength: In DIW, the prevailing method is to over-extrude material at the interface to enhance mechanical interlocking, which lacks precision and can lead to material waste [156, 166]. In DLP, the light absorption of magnetic fillers reduces crosslinking at the material interface, weakening adhesion [70, 71]. As a result, current research has largely been limited to interlayer multi-material integration rather than same-layer integration [80, 154, 155, 176]. Future improvements may include developing interface-bonding enhanced materials for DIW to ensure strong adhesion between dissimilar materials, and adopting overlapping exposure in DLP (where projection patterns for different material regions in the same layer overlap at their boundaries) to improve crosslinking density and interface strength. Second, the lack of multi-material printing systems: current multi-material DLP 3D printing workflows rely on manual resin switching and part or vat cleaning, which are inefficient and inconsistent [80, 176]. The development of automated material switching and cleaning systems will be essential for enabling high-efficiency, repeatable, and scalable multi-material DLP 3D printing. In addition, future MF3DP systems may increasingly

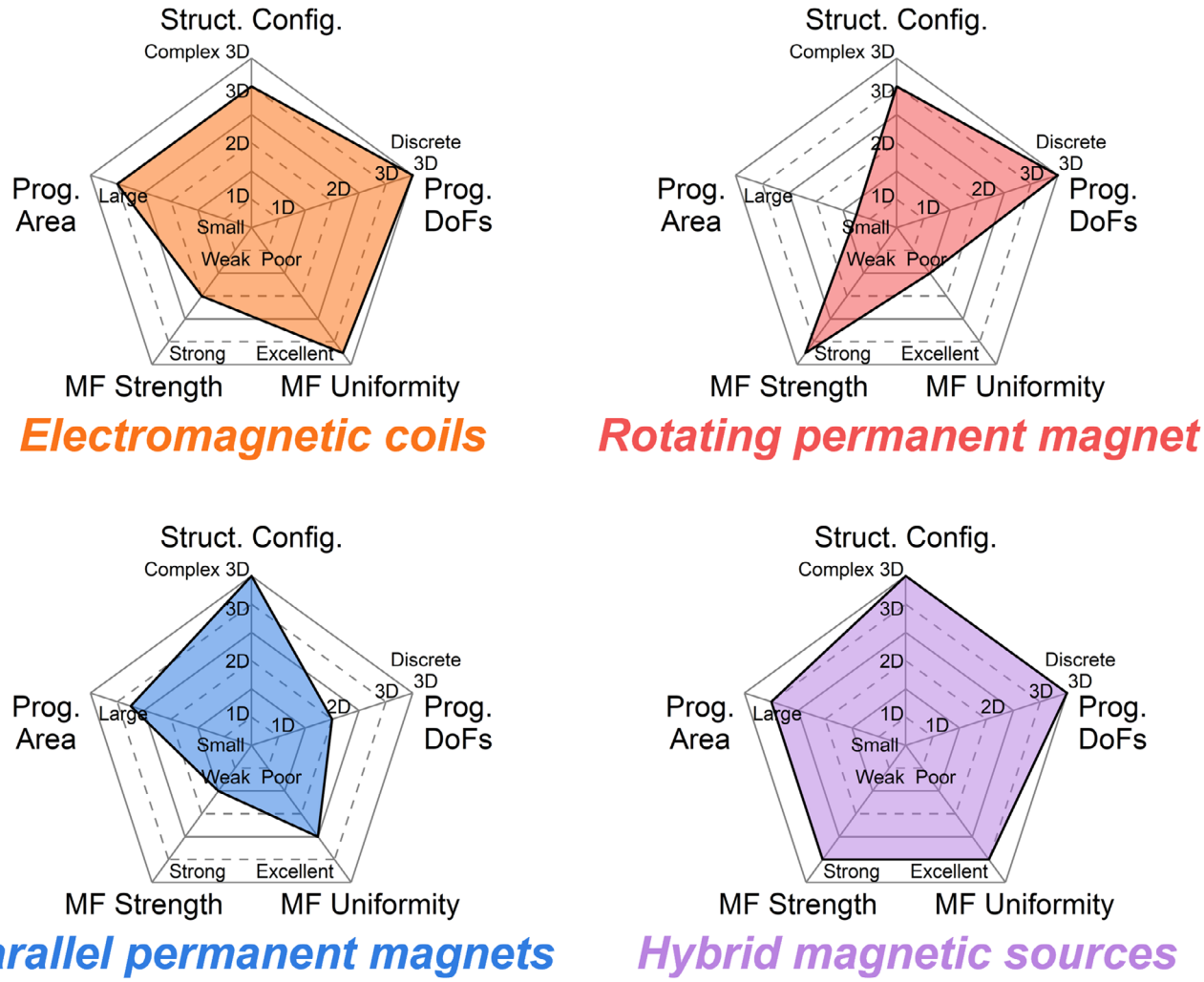

FIGURE 20 | Comparison of manufacturing capabilities and programming field performance of DLP-based MF3DP systems using different magnetic sources. The radar plots compare structural configuration (Struct. Config.; 1D to complex 3D), programming area (Prog. Area; small to large), programming degrees of freedom (Prog. DoFs; 1D to discrete 3D), magnetic field strength (MF Strength; weak to strong), and magnetic field uniformity (MF Uniformity; poor to excellent).

benefit from in situ characterization and process monitoring strategies, including real-time observation of particle alignment, printing geometry, and curing state during fabrication. Such capabilities may provide valuable feedback for improving printing reliability, magnetic programming accuracy, and manufacturing consistency of complex MSM structures. As multi-material MSM structures become increasingly accessible, their structural, material, and functional design space will also expand substantially, thereby calling for more advanced computational design strategies.

4.2 | Computational Modeling, Inverse Design, and ML-Assisted Optimization

As MSM structures are expected to integrate increasingly diverse functions and perform more complex tasks, their structural and functional complexity is also continuously increasing [27, 77, 134]. The field is moving beyond simple beams, films, and single-function actuators toward more sophisticated structures that combine complex 3D geometries, heterogeneous material distributions, and multiple coupled functionalities. Under such circumstances, the design of MSM structures can no longer rely mainly on empirical trial-and-error approaches. For relatively simple structures and loading conditions, analytical models and forward simulations are often sufficient to describe magnetic actuation behaviors [32, 80]. However, for complex 3D structures, hybrid materials, and multifunctional devices, the overall response is governed by the coupled effects of geometry, material distribution, magnetization profile, and external magnetic fields, which greatly increases the design complexity [26, 177]. Therefore, establishing computational modeling frameworks that can accurately predict the relationship among structural geometry, magnetic programming, and functional response is becoming increasingly important [77].

Beyond forward prediction, inverse design is expected to become a key direction for future MSM research [46, 78, 178]. In such a design paradigm, the desired deformed shape, actuation mode, or functional output is specified first, and the corresponding structural geometry, material layout, and 3D magnetization profile are then determined computationally. This strategy is particularly

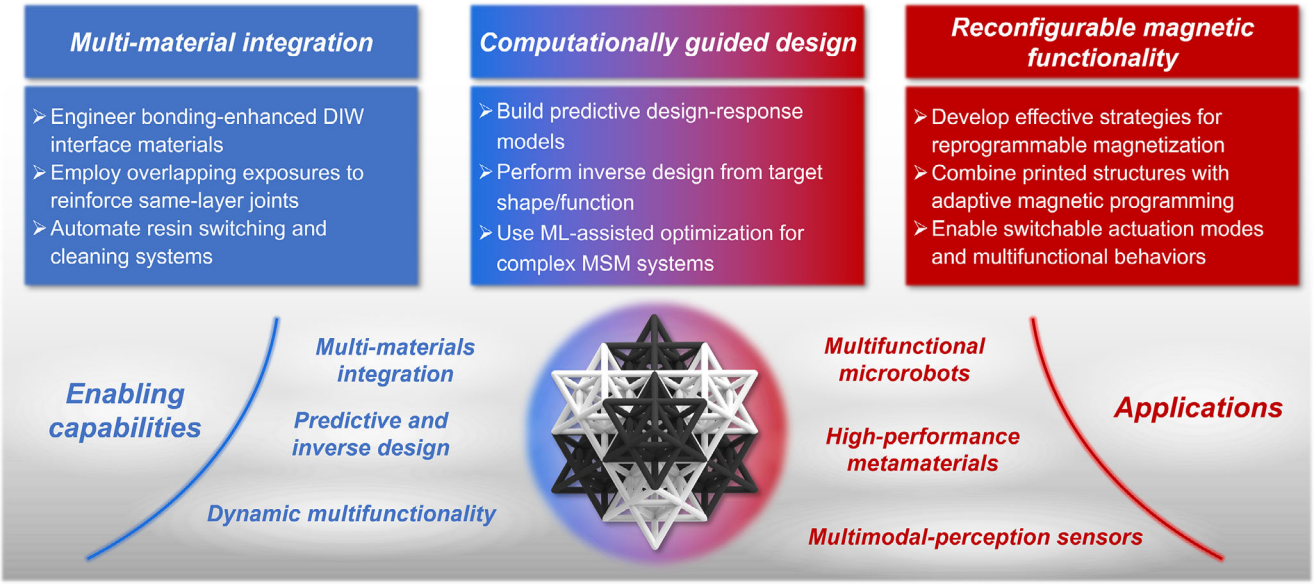

FIGURE 21 | Perspective on the future development of 3D printing of MSMs for advanced structures and devices, highlighting three key directions: multi-material integration, computationally guided design, and reconfigurable magnetic functionality, together with their enabling capabilities and potential applications.

valuable for 4D printing of MSMs, where structural geometry, material distribution, magnetization profile, and external field conditions often need to be determined in a coupled manner, making the design process much more complex than that of conventional soft actuators. In recent years, optimization algorithms and machine-learning (ML)-assisted design methods have shown increasing potential in addressing such problems, especially for structures involving nonlinear deformation, multiple material phases, or strongly coupled geometric, magnetic, and material parameters [77, 78, 178]. Future research should therefore focus on integrating computational modeling, inverse design, and data-driven optimization with MSM manufacturing processes, so that complex MSM structures and devices can be designed more efficiently and realized more reliably.

4.3 | Reconfigurable Magnetization for Dynamic and Multifunctional MSM Structures

As MSM structures are being developed toward higher functional integration and more demanding operational tasks, their magnetic programming is also expected to evolve beyond fixed magnetic configurations [10]. Most MSM structures reported to date are based on fixed magnetization profiles established either after fabrication [1] or during printing [32]. This strategy has enabled a wide range of magnetic actuation behaviors and functional device demonstrations [22, 29, 80]. However, once the magnetization profile is fixed, the accessible deformation mode and device function are also largely predetermined, which limits the adaptability, reusability, and task versatility of the structure in changing environments. Therefore, beyond improving the capability to fabricate structures with increasingly complex static magnetic patterns, a more forward-looking direction is to develop MSM structures whose magnetic states can be reconfigured after fabrication in a controllable and reversible manner [10, 76, 101, 139, 179, 180].

The combination of 3D printing and reconfigurable magnetization may open a new route toward dynamic and multifunctional MSM structures. In such a paradigm, 3D printing provides the initial geometry and material distribution of the structure, while reconfigurable magnetization enables the same printed structure to perform multiple actuation modes or functional tasks under identical or simplified external magnetic field conditions [10, 76, 181]. This concept may significantly broaden the capability of MSM structures from preprogrammed single-function designs to adaptive structures with switchable, reprogrammable, or even real-time tunable behaviors. Future progress will depend less on simply creating more complex fixed magnetic patterns and more on developing effective reconfigurable magnetization strategies. Such advances will be essential for transforming 3D-printed MSM structures from preprogrammed single-function designs into more dynamic, adaptive, and multifunctional designs.

Acknowledgements

Q.G. acknowledges the financial support from the National Natural Science Foundation of China (No. 12472152) and the Department of Science and Technology of Guangdong Province (No. 2019QN01Z438).

Conflicts of Interest

The authors declare no conflicts of interest.

Data Availability Statement

The data that support the findings of this study are available from the corresponding author upon reasonable request.

References

1. W. Hu, G. Z. Lum, M. Mastrangeli, and M. Sitti, "Small-Scale Soft-Bodied Robot With Multimodal Locomotion," *Nature* 554 (2018): 81–85.

2. L. Zhang, J. J. Abbott, L. Dong, B. E. Kratochvil, D. Bell, and B. J. Nelson, "Artificial Bacterial Flagella: Fabrication and Magnetic Control," *Applied Physics Letters* 94 (2009): 064107 .

3. R. M. Erb, R. Libanori, N. Rothfuchs, and A. R. Studart, "Composites Reinforced in Three Dimensions by Using Low Magnetic Fields," *Science* 335 (2012): 199–204.

4. J. Billaud, F. Bouville, T. Magrini, C. Villevieille, and A. R. Studart, "Magnetically Aligned Graphite Electrodes for High-Rate Performance Li-Ion Batteries," *Nature Energy* 1 (2016): 16097.

5. J. Ammann, P. Ruch, B. Michel, and A. R. Studart, "High-Power Adsorption Heat Pumps Using Magnetically Aligned Zeolite Structures," *ACS Applied Materials & Interfaces* 11 (2019): 24037–24046.

6. N. Xia, D. Jin, C. Pan, et al., "Dynamic Morphological Transformations in Soft Architected Materials via Buckling Instability Encoded Heterogeneous Magnetization," *Nature Communications* 13 (2022): 7514.

7. S. Jeon, S. Kim, S. Ha, et al., "Magnetically Actuated Microrobots as a Platform for Stem Cell Transplantation," *Science Robotics* 4 (2019): aav4317.

8. L. Su, D. Jin, Y. Wang, et al., "Modularized Microrobot With Lock-and-Detachable Modules for Targeted Cell Delivery in Bile Duct," *Science Advances* 9 (2023): adj0883.

9. S. Tottori, L. Zhang, F. Qiu, K. K. Krawczyk, A. Franco-Obregon, and B. J. Nelson, "Magnetic Helical Micromachines: Fabrication, Controlled Swimming, and Cargo Transport," *Advanced Materials* 24 (2012): 811–816.

10. X. Bao, F. Wang, J. Zhang, et al., "Real-Time In Situ Magnetization Reprogramming for Soft Robotics," *Nature* 645 (2025): 375–384.

11. T. Zhang, F. Manshaii, C. R. Bowen, et al., "A Flexible Pressure Sensor Array for Self-Powered Identity Authentication During Typing," *Science Advances* 11 (2025): ads2297.

12. H. Wu, X. Zhang, Z. Ma, et al., "A Material Combination Concept to Realize 4D Printed Products With Newly Emerging Property/Functionality," *Advanced Science* 7 (2020): 1903208.

13. X. Zhao, Y. Zhou, J. Xu, et al., "Soft Fibers With Magnetoelasticity for Wearable Electronics," *Nature Communications* 12 (2021): 6755.

14. L. Ren, B. Li, Z. Song, Q. Liu, L. Ren, and X. Zhou, "Bioinspired Fiber-Regulated Composite With Tunable Permanent Shape and Shape Memory Properties via 3d Magnetic Printing," *Composites Part B: Engineering* 164 (2019): 458–466.

15. C. Li, G. C. Lau, H. Yuan, et al., "Fast and Programmable Locomotion of Hydrogel-Metal Hybrids Under Light and Magnetic Fields," *Science Robotics* 5 (2020): abb9822.

16. S. Safaee and R. K. Chen, "Development of a Design and Characterization Framework for Fabrication of Functionally Graded Materials Using Magnetic Field-Assisted Digital Light Processing Stereolithography," *Journal of Manufacturing Processes* 67 (2021): 314–324.

17. S. Safaee, A. Otero, M. Fei, T. Liu, J. Zhang, and R. K. Chen, "Particle-Resin Systems for Additive Manufacturing of Rigid and Elastic Magnetic Polymeric Composites," *Additive Manufacturing* 51 (2022): 102587.

18. I. Mattich, J. Sendra, H. Galinski, et al., "Magnetic Manipulation of Superparamagnetic Colloids in Droplet-Based Optical Devices," *Advanced Optical Materials* 11 (2023): 2300734.

19. A. Calikoglu, F. Lux, Y. Taege, H. Zappe, and Ç. Ataman, "3D Nano-Printed Bistable Microlens Actuator for Reconfigurable Micro-Optical Systems," *Advanced Functional Materials* 34 (2024): 2408867.

20. J. Zhao, C. Xin, J. Zhu, et al., "Insect-Scale Biped Robots Based on Asymmetrical Friction Effect Induced by Magnetic Torque," *Advanced Materials* 36 (2024): 2312655.

21. T. Chen, M. Pauly, and P. M. Reis, "A Reprogrammable Mechanical Metamaterial With Stable Memory," *Nature* 589 (2021): 386–390.

22. D. Tang, C. Zhang, C. Pan, et al., "Bistable Soft Jumper Capable of Fast Response and High Takeoff Velocity," *Science Robotics* 9 (2024): adm8484.

23. Z. Ren, R. Zhang, R. H. Soon, et al., "Soft-Bodied Adaptive Multimodal Locomotion Strategies in Fluid-Filled Confined Spaces," *Science Advances* 7 (2021): abh2022.

24. S. Yi, L. Wang, Z. Chen, et al., "High-Throughput Fabrication of Soft Magneto-Origami Machines," *Nature Communications* 13 (2022): 4177.

25. G. Zhu, Y. Hou, N. Xia, et al., "Fully Recyclable, Healable, Soft, and Stretchable Dynamic Polymers for Magnetic Soft Robots," *Advanced Functional Materials* 33 (2023): 2300888.

26. J. Zhang, Z. Ren, W. Hu, et al., "Voxelated Three-Dimensional Miniature Magnetic Soft Machines via Multimaterial Heterogeneous Assembly," *Science Robotics* 6 (2021): abf0112.

27. Y. Dong, L. Wang, N. Xia, et al., "Untethered Small-Scale Magnetic Soft Robot With Programmable Magnetization and Integrated Multifunctional Modules," *Science Advances* 8 (2022): abn8932.

28. C. Hong, Z. Ren, C. Wang, et al., "Magnetically Actuated Gearbox for the Wireless Control of Millimeter-Scale Robots," *Science Robotics* 7 (2022): abo4401.

29. N. Xia, B. Jin, D. Jin, et al., "Decoupling and Reprogramming the Wiggling Motion of Midge Larvae Using a Soft Robotic Platform," *Advanced Materials* 34 (2022): 2109126.

30. X. Liu, L. Wang, Y. Xiang, et al., "Magnetic Soft Microfiberbots for Robotic Embolization," *Science Robotics* 9 (2024): adh2479.

31. Y. Kim, G. A. Parada, S. Liu, and X. Zhao, "Ferromagnetic Soft Continuum Robots," *Science Robotics* 4 (2019): aax7329.

32. Y. Kim, H. Yuk, R. Zhao, S. A. Chester, and X. Zhao, "Printing Ferromagnetic Domains for Untethered Fast-Transforming Soft Materials," *Nature* 558 (2018): 274–279.

33. T. Xu, J. Zhang, M. Salehizadeh, O. Onaizah, and E. Diller, "Millimeter-scale Flexible Robots with Programmable Three-dimensional Magnetization and Motions," *Science Robotics* 4 (2019): aav4494.

34. Q. Ge, Z. Li, Z. Wang, et al., "Projection Micro Stereolithography Based 3D Printing and Its Applications," *International Journal of Extreme Manufacturing* 2 (2020): 022004.

35. L. Y. Zhou, J. Fu, and Y. He, "A Review of 3D Printing Technologies for Soft Polymer Materials," *Advanced Functional Materials* 30 (2020): 2000187.

36. Q. Ge, B. Jian, and H. Li, "Shaping Soft Materials via Digital Light Processing-Based 3D Printing: A Review," *Forces in Mechanics* 6 (2022): 100074.

37. Q. Ge, Z. Chen, J. Cheng, et al., "3D Printing of Highly Stretchable Hydrogel With Diverse UV Curable Polymers," *Science Advances* 7 (2021): aba4261.

38. Q. Ge, C. K. Dunn, H. J. Qi, and M. L. Dunn, "Active Origami by 4D Printing," *Smart Materials and Structures* 23 (2014): 094007.

39. Q. Ge, A. H. Sakhaei, H. Lee, C. K. Dunn, N. X. Fang, and M. L. Dunn, "Multimaterial 4D Printing With Tailorable Shape Memory Polymers," *Scientific Reports* 6 (2016): 31110.

40. B. Zhang, H. Li, J. Cheng, et al., "Mechanically Robust and UV-Curable Shape-Memory Polymers for Digital Light Processing Based 4D Printing," *Advanced Materials* 33 (2021): 2101298.

41. J. Cheng, S. Yu, R. Wang, and Q. Ge, "Digital Light Processing Based Multimaterial 3D Printing: Challenges, Solutions and Perspectives," *International Journal of Extreme Manufacturing* 6 (2024): 042006.

42. H. Ye, C. Li, S. Yu, et al., "Adaptive Energy Dissipator With Compression-to-Tension Design," *Advanced Functional Materials* 36 (2025): 21393.

43. A. Heiden, D. Preninger, L. Lehner, et al., "3D Printing of Resilient Biogels for Omnidirectional and Exteroceptive Soft Actuators," *Science Robotics* 7 (2022): abk2119.

44. Q. Liu, H. Ye, J. Cheng, et al., "Stiffness-Tunable Origami Structures via Multimaterial Three-Dimensional Printing," *Acta Mechanica Solida Sinica* 36 (2023): 582–593.

45. H. Ye, Q. Liu, J. Cheng, et al., "Multimaterial 3D Printed Self-Locking Thick-Panel Origami Metamaterials," *Nature Communications* 14 (2023): 1607.

46. L. Jin, S. Yu, J. Cheng, et al., "Machine Learning Driven Forward Prediction and Inverse Design for 4D Printed Hierarchical Architecture With Arbitrary Shapes," *Applied Materials Today* 40 (2024): 102373.

47. M. A. Skylar-Scott, J. Mueller, C. W. Visser, and J. A. Lewis, "Voxelated Soft Matter via Multimaterial Multinozzle 3D Printing," *Nature* 575 (2019): 330–335.

48. J. A. Lewis, "Direct Ink Writing of 3D Functional Materials," *Advanced Functional Materials* 16 (2006): 2193–2204.

49. L. Li, J. Meng, X. Bao, et al., "Direct-Ink-Write 3D Printing of Programmable Micro-Supercapacitors From MXene-Regulating Conducting Polymer Inks," *Advanced Energy Materials* 13 (2023): 2203683.

50. C. Bader, D. Kolb, J. C. Weaver, et al., "Making Data Matter: Voxel Printing for the Digital Fabrication of Data Across Scales and Domains," *Science Advances* 4 (2018): aas8652.

51. Q. Ge, H. J. Qi, and M. L. Dunn, "Active Materials by Four-Dimension Printing," *Applied Physics Letters* 103 (2013): 131901.

52. Y. F. Zhang, N. Zhang, H. Hingorani, et al., "Fast-Response, Stiffness-Tunable Soft Actuator by Hybrid Multimaterial 3D Printing," *Advanced Functional Materials* 29 (2019): 1806698.

53. Z. C. Eckel, C. Zhou, J. H. Martin, A. J. Jacobsen, W. B. Carter, and T. A. Schaedler, "Additive Manufacturing of Polymer-Derived Ceramics," *Science* 351 (2016): 58–62.

54. M. Shusteff, A. E. Browar, B. E. Kelly, et al., "One-Step Volumetric Additive Manufacturing of Complex Polymer Structures," *Science Advances* 3 (2017): aao5496.

55. J. Wang, A. Goyanes, S. Gaisford, and A. W. Basit, "Stereolithographic (SLA) 3D Printing of Oral Modified-Release Dosage Forms," *International Journal of Pharmaceutics* 503 (2016): 207–212.

56. Y. A. Orozco-Osorio, A. V. Gaita-Anturi, C. P. Ossa-Orozco, et al., "Utilization of Additive Manufacturing Techniques for the Development of a Novel Scaffolds With Magnetic Properties for Potential Application in Enhanced Bone Regeneration," *Small* 20 (2024): 2402419.

57. X. Zheng, H. Lee, T. H. Weisgraber, et al., "Ultralight, Ultrastiff Mechanical Metamaterials," *Science* 344 (2014): 1373–1377.

58. J. Cheng, R. Wang, Z. Sun, et al., "Centrifugal Multimaterial 3D Printing of Multifunctional Heterogeneous Objects," *Nature Communications* 13 (2022): 7931.

59. X. He, B. Zhang, Q. Liu, et al., "Highly Conductive and Stretchable Nanostructured Ionogels for 3D Printing Capacitive Sensors With Superior Performance," *Nature Communications* 15 (2024): 6431.

60. H. Li, B. Zhang, H. Ye, et al., "Reconfigurable 4D Printing via Mechanically Robust Covalent Adaptable Network Shape Memory Polymer," *Science Advances* 10 (2024): adl4387.

61. H. Li, Z. Chen, S. Yu, B. Jian, H. Yin, and Q. Ge, "Selective near-infrared Laser Programming for Shape-memory Polymer–carbon Nanotube Composite Material 4D Printing," *Programmable Materials* 2 (2024): 6.

62. L. Jin, S. Yu, J. Cheng, et al., "Machine Learning Powered Inverse Design for Strain Fields of Hierarchical Architectures," *Composites Part B: Engineering* 299 (2025): 112372.

63. R. Wang, C. Yuan, J. Cheng, et al., "Direct 4D Printing of Ceramics Driven by Hydrogel Dehydration," *Nature Communications* 15 (2024): 758.

64. X. Wen, B. Zhang, W. Wang, et al., "3D-printed Silica with Nanoscale Resolution," *Nature Materials* 20 (2021): 1506–1511.

65. B. Jian, H. Li, X. He, R. Wang, H. Y. Yang, and Q. Ge, "Two-photon Polymerization-based 4D Printing and Its Applications," *International Journal of Extreme Manufacturing* 6 (2023): 012001.

66. S. Kawata, H.-B. Sun, T. Tanaka, and K. Takada, "Finer Features for Functional Microdevices," *Nature* 412 (2001): 697–698.

67. J. M. Williams, A. Adewunmi, R. M. Schek, et al., "Bone Tissue Engineering Using Polycaprolactone Scaffolds Fabricated via Selective Laser Sintering," *Biomaterials* 26 (2005): 4817–4827.

68. S. Eshraghi and S. Das, "Mechanical and Microstructural Properties of Polycaprolactone Scaffolds With One-Dimensional, Two-Dimensional, and Three-Dimensional Orthogonally Oriented Porous Architectures Produced by Selective Laser Sintering," *Acta Biomaterialia* 6 (2010): 2467–2476.

69. J. P. Kruth, P. Mercelis, J. Van Vaerenbergh, L. Froyen, and M. Rombouts, "Binding Mechanisms in Selective Laser Sintering and Selective Laser Melting," *Rapid Prototyping Journal* 11 (2005): 26–36.

70. Z. Huang, G. Shao, D. Zhou, X. Deng, J. Qiao, and L. Li, "3D Printing of High-Precision and Ferromagnetic Functional Devices," *International Journal of Extreme Manufacturing* 5 (2023): 035501.

71. A. Zhou, C. Xu, P. Kanitthamniyom, et al., "Magnetic Soft Millirobots 3D Printed by Circulating Vat Photopolymerization to Manipulate Droplets Containing Hazardous Agents for In Vitro Diagnostics," *Advanced Materials* 34 (2022): 2200061.

72. Z. Chen, D. Zhao, B. Liu, et al., "3D Printing of Multifunctional Hydrogels," *Advanced Functional Materials* 29 (2019): 1900971.

73. Z. Li, D. Weng, L. Chen, Y. Ma, Z. Wang, and J. Wang, "Enhanced Digital Light Processing-Based One-Step 3-Dimensional Printing of Multifunctional Magnetic Soft Robot," *Cyborg and Bionic Systems* 6 (2025): 0215.

74. Z. Ren and M. Sitti, "Design and Build of Small-Scale Magnetic Soft-Bodied Robots With Multimodal Locomotion," *Nature Protocols* 19 (2024): 441–486.

75. G. Z. Lum, Z. Ye, X. Dong, et al., "Shape-Programmable Magnetic Soft Matter," *Proceedings of the National Academy of Sciences* 113 (2016): E6007.

76. Y. Alapan, A. C. Karacakol, S. N. Guzelhan, I. Isik, and M. Sitti, "Reprogrammable Shape Morphing of Magnetic Soft Machines," *Science Advances* 6 (2020): abc6414.

77. A. C. Karacakol, Y. Alapan, S. O. Demir, and M. Sitti, "Data-Driven Design of Shape-Programmable Magnetic Soft Materials," *Nature Communications* 16 (2025): 2946.

78. N. Xia, D. Jin, Z. Yang, et al., "Inverse Programming of Ferromagnetic Domains for 3D Curved Surfaces of Soft Materials," *Nature Synthesis* 4 (2025): 642–654.

79. J. L. Kricke, I. Yusnila Khairani, B. B. Beele, et al., "4D Printing of Magneto-Responsive Polymer Structures by Masked Stereolithography for Miniaturised Actuators," *Virtual and Physical Prototyping* 18 (2023): 2251017.

80. X. Meng, S. Li, X. Shen, C. Tian, L. Mao, and H. Xie, "Programmable Spatial Magnetization Stereolithographic Printing of Biomimetic Soft Machines With Thin-Walled Structures," *Nature Communications* 15 (2024): 10442.

81. S. Li, X. Meng, X. Shen, J. Wang, and H. Xie, "Development of a Photo-Curing 3D Printer for Fabrication of Small-Scale Soft Robots With Programming Spatial Magnetization," *IEEE Robotics and Automation Letters* 10 (2025): 2766–2773.

82. M. H. D. Ansari, V. Iacovacci, S. Pane, et al., "3D Printing of Small-Scale Soft Robots With Programmable Magnetization," *Advanced Functional Materials* 33 (2023): 2211918.

83. Y. Kim and X. Zhao, "Magnetic Soft Materials and Robots," *Chemical Reviews* 122 (2022): 5317–5364.

84. C. Zhang, X. Li, L. Jiang, et al., "3D Printing of Functional Magnetic Materials: From Design to Applications," *Advanced Functional Materials* 31 (2021): 2102777.

85. N. Xia, D. Jin, and L. Zhang, "Magnetic Soft Matter Toward Programmable and Multifunctional Miniature Machines," *Accounts of Materials Research* 5 (2024): 173–183.

86. X. Wei, M.-L. Jin, H. Yang, X.-X. Wang, Y.-Z. Long, and Z. Chen, "Advances in 3D Printing of Magnetic Materials: Fabrication, Properties, and Their Applications," *Journal of Advanced Ceramics* 11 (2022): 665–701.

87. Y. Deng, Y. Zhao, J. Zhang, T. Arai, Q. Huang, and X. Liu, "Fabrication of Magnetic Microrobots by Assembly," *Advanced Intelligent Systems* 6 (2024): 2300471.

88. H. Zhai, X. Li, S. Yu, et al., "Review on the 3D Printing Technology and Application of Magnetic Materials: Material-Process-Structure-Application," *Composites Part B: Engineering* 298 (2025): 112387.

89. B. Rezaei, H. E. J. Moni, I. H. Karampelas, et al., "Additive Manufacturing of Magnetic Materials for Energy, Environment, Healthcare, and Industry Applications," *Advanced Functional Materials* 35 (2025): 2416823.

90. O. Gutfleisch, "Controlling the Properties of High Energy Density Permanent Magnetic Materials by Different Processing Routes," *Journal of Physics D: Applied Physics* 33 (2000): R157–R172.

91. O. Gutfleisch, M. A. Willard, E. Bruck, C. H. Chen, S. G. Sankar, and J. P. Liu, "Magnetic Materials and Devices for the 21st Century: Stronger, Lighter, and More Energy Efficient," *Advanced Materials* 23 (2011): 821–842.

92. K. M. Krishnan, *Fundamentals and Applications of Magnetic Materials* (Oxford University Press, 2016).

93. M. D. Nguyen, H.-V. Tran, S. Xu, and T. R. Lee, "Fe_3O_4 Nanoparticles: Structures, Synthesis, Magnetic Properties, Surface Functionalization, and Emerging Applications," *Applied Sciences* 11 (2021): 11301.

94. A. Rajan, M. Sharma, and N. K. Sahu, "Assessing Magnetic and Inductive Thermal Properties of Various Surfactants Functionalised Fe_3O_4 Nanoparticles for Hyperthermia," *Scientific Reports* 10 (2020): 15045.

95. J. He, Y. Sun, Q. Gao, et al., "Gelatin Methacryloyl Hydrogel, From Standardization, Performance, to Biomedical Application," *Advanced Healthcare Materials* 12 (2023): 2300395.

96. A. Motealleh and N. S. Kehr, "Nanocomposite Hydrogels and Their Applications in Tissue Engineering," *Advanced Healthcare Materials* 6 (2017): 1600938.

97. F. Canfarotta and S. A. Piletsky, "Engineered Magnetic Nanoparticles for Biomedical Applications," *Advanced Healthcare Materials* 3 (2014): 160–175.

98. H. Y. Yang, Y. Li, and D. S. Lee, "Functionalization of Magnetic Nanoparticles With Organic Ligands Toward Biomedical Applications," *Advanced NanoBiomed Research* 1 (2021): 2000043.

99. G. Chen, T. Chung, Z. Liu, et al., "Hemodynamics-Driven Magnetoelastic Vascular Grafts for Stenosis Diagnosis," *Nature Biotechnology* 44 (2026): 406–417.

100. G. Chen, W. J. Kim, Y. Yang, et al., "Self-Powered In-Stent Restenosis Diagnosis via Magnetoelastic Stents," *Nature Cardiovascular Research* 5 (2026): 155–167.

101. C. W. Zhang, X. P. Hao, W. Zou, et al., "Supramolecular Hydrogel Actuators With Reprogrammable Magnetic Orientation by Locally Mediated Viscoelasticity and Pinning Force," *Science Advances* 11 (2025): adw0500.

102. J. C. Breger, C. Yoon, R. Xiao, et al., "Self-Folding Thermo-Magnetically Responsive Soft Microgrippers," *ACS Applied Materials & Interfaces* 7 (2015): 3398–3405.

103. X. Du, H. Cui, T. Xu, et al., "Reconfiguration, Camouflage, and Color-Shifting for Bioinspired Adaptive Hydrogel-Based Millirobots," *Advanced Functional Materials* 30 (2020): 1909202.

104. X. Hu, G. Nian, X. Liang, et al., "Adhesive Tough Magnetic Hydrogels With High Fe_3O_4 Content," *ACS Applied Materials & Interfaces* 11 (2019): 10292–10300.

105. C. Mayer, V. Cabuil, T. Lalot, and R. Thouvenot, "Magnetic Nanoparticles Trapped in pH 7 Hydrogels as a Tool to Characterize the Properties of the Polymeric Network," *Advanced Materials* 12 (2000): 417–420.

106. B. Sun, R. Jia, H. Yang, et al., "Magnetic Arthropod Millirobots Fabricated by 3D-Printed Hydrogels," *Advanced Intelligent Systems* 4 (2022): 2100139.

107. X. Liu, Y. Yang, M. E. Inda, et al., "Magnetic Living Hydrogels for Intestinal Localization, Retention, and Diagnosis," *Advanced Functional Materials* 31 (2021): 2010918.

108. P. Reséndiz-Hernández, O. Rodríguez-Fernández, and L. Garcia-Cerda, "Synthesis of Poly(vinyl alcohol)–Magnetite Ferrogel Obtained by Freezing–Thawing Technique," *Journal of Magnetism and Magnetic Materials* 320 (2008): e373–e376.

109. H. Lin, Y. Watanabe, M. Kimura, K. Hanabusa, and H. Shirai, "Preparation of Magnetic Poly(vinyl alcohol) (PVA) Materials by In Situ Synthesis of Magnetite in a PVA Matrix," *Journal of Applied Polymer Science* 87 (2003): 1239–1247.

110. M. Zrinyi, L. Barsi, and A. Büki, "Ferrogel: A New Magneto-Controlled Elastic Medium," *Polymer Gels and Networks* 5 (1997): 415–427.

111. S. Ghosh and T. Cai, "Controlled Actuation of Alternating Magnetic Field-Sensitive Tunable Hydrogels," *Journal of Physics D: Applied Physics* 43 (2010): 415504.

112. J. Tang, Q. Yin, Y. Qiao, and T. Wang, "Shape Morphing of Hydrogels in Alternating Magnetic Field," *ACS Applied Materials & Interfaces* 11 (2019): 21194–21200.

113. C. A. Cezar, S. M. Kennedy, M. Mehta, et al., "Biphasic Ferrogels for Triggered Drug and Cell Delivery," *Advanced Healthcare Materials* 3 (2014): 1869–1876.

114. X. Zhao, J. Kim, C. A. Cezar, et al., "Active Scaffolds for On-Demand Drug and Cell Delivery," *Proceedings of the National Academy of Sciences* 108 (2011): 67–72.

115. N. J. François, S. Allo, S. E. Jacobo, and M. E. Daraio, "Composites of Polymeric Gels and Magnetic Nanoparticles: Preparation and Drug Release Behavior," *Journal of Applied Polymer Science* 105 (2007): 647.

116. H. K. Kim, H. S. Kim, and Y.-K. Kim, "Stiffness Control of Magnetorheological Gels for Adaptive Tunable Vibration Absorber," *Smart Materials and Structures* 26 (2016): 015016.

117. T. Mitsumata and N. Abe, "Giant and Reversible Magnetorheology of Carrageenan/Iron Oxide Magnetic Gels," *Smart Materials and Structures* 20 (2011): 124003.

118. J. Ikeda, D. Takahashi, M. Watanabe, M. Kawai, and T. Mitsumata, "Particle Size in Secondary Particle and Magnetic Response for Carrageenan Magnetic Hydrogels," *Gels* 5 (2019): 39.

119. T. Mitsumata, A. Honda, H. Kanazawa, and M. Kawai, "Magnetically Tunable Elasticity for Magnetic Hydrogels Consisting of Carrageenan and Carbonyl Iron Particles," *The Journal of Physical Chemistry B* 116 (2012): 12341–12348.

120. M. Ha, G. S. Cañón Bermúdez, J. A. C. Liu, et al., "Reconfigurable Magnetic Origami Actuators With On-Board Sensing for Guided Assembly," *Advanced Materials* 33 (2021): 2008751.

121. J. A. C. Liu, E. E. Evans, and J. B. Tracy, "Photothermally Reconfigurable Shape Memory Magnetic Cilia," *Advanced Materials Technologies* 5 (2020): 2000147.

122. J. A.-C. Liu, J. H. Gillen, S. R. Mishra, E. E. Evans, and J. B. Tracy, "Photothermally and Magnetically Controlled Reconfiguration of Polymer Composites for Soft Robotics," *Science Advances* 5 (2019): aaw2897.

123. Q. Ze, X. Kuang, S. Wu, et al., "Magnetic Shape Memory Polymers With Integrated Multifunctional Shape Manipulation," *Advanced Materials* 32 (2020): 1906657.

124. R. S. Kularatne, H. Kim, J. M. Boothby, and T. H. Ware, "Liquid Crystal Elastomer Actuators: Synthesis, Alignment, and Applications," *Journal of Polymer Science Part B: Polymer Physics* 55 (2017): 395–411.

125. Y. Ji, J. E. Marshall, and E. M. Terentjev, "Nanoparticle-Liquid Crystalline Elastomer Composites," *Polymers* 4 (2012): 316–340.

126. P. Wu, T. Yu, L. Zhao, and M. Chen, "Magnetic Field-Assisted 3D Printing of Magnetic Self-Powered Sensors," *Virtual and Physical Prototyping* 19 (2024): 2391487.

127. H. Wu, R. Luo, Z. Li, et al., "Additively Manufactured Flexible Liquid Metal–Coated Self-Powered Magnetoelectric Sensors With High Design Freedom," *Advanced Materials* 36 (2024): 2307546.

128. Y. Yan, Z. Hu, Z. Yang, et al., "Soft Magnetic Skin for Super-resolution Tactile Sensing With Force Self-Decoupling," *Science Robotics* 6 (2021): abc8801.

129. H. Dai, C. Zhang, C. Pan, et al., "Split-Type Magnetic Soft Tactile Sensor With 3D Force Decoupling," *Advanced Materials* 36 (2024): 2310145.

130. T. E. Greenwood, B. Elder, M. N. Hasan, et al., "Soft Multistable Magnetic-Responsive Metamaterials," *Science Advances* 11 (2025): adu3749.

131. X. Liu, H. Tang, N. Li, et al., "Miniature Magneto-Ultrasonic Machines for Wireless Robotic Sensing and Manipulation," *Science Robotics* 10 (2025): adu4851.

132. J. Han, S. Wang, Z. Zheng, et al., "Template-Free 3D Programmable Magnetization of Soft Millirobots Induced by Interlayer Stress," *Proceedings of the National Academy of Sciences* 122 (2025): 2426846122.

133. J. Yoo, G. Chung, and Y. Park, "Bio-Inspired, Miniaturized Magnetic Heart Valve System for Superior Performance Cardiovascular Simulator," *Advanced Materials* 37 (2025): 2419504.

134. C. Hong, Y. Wu, C. Wang, et al., "Wireless Flow-Powered Miniature Robot Capable of Traversing Tubular Structures," *Science Robotics* 9 (2024): adi5155.

135. Q. Peng, S. Wang, J. Han, et al., "Thermal and Magnetic Dual-Responsive Catheter-Assisted Shape Memory Microrobots for Multistage Vascular Embolization," *Research* 7 (2024): 0339.

136. B. Wang, J. Shen, C. Huang, et al., "Magnetically Driven Biohybrid Blood Hydrogel Fibres for Personalized Intracranial Tumour Therapy Under Fluoroscopic Tracking," *Nature Biomedical Engineering* 9 (2025): 1471–1485.

137. J. Cañada, H. Kim, and L. F. Velásquez-García, "Three-Dimensional, Soft Magnetic-Cored Solenoids via Multi-Material Extrusion," *Virtual and Physical Prototyping* 19 (2024): 2310046.

138. X. Cao, S. Xuan, S. Sun, Z. Xu, J. Li, and X. Gong, "3D Printing Magnetic Actuators for Biomimetic Applications," *ACS Applied Materials & Interfaces* 13 (2021): 30127–30136.

139. Y. Zhang, X. Zhu, H. Chen, et al., "Integrated 3D Printing of Reconfigurable Soft Machines With Magnetically Actuated Crease-Assisted Pixelated Structures," *Additive Manufacturing* 94 (2024): 104513.

140. H. Liu, F. Wang, W. Wu, X. Dong, and L. Sang, "4D Printing of Mechanically Robust PLA/TPU/Fe_3O_4 Magneto-Responsive Shape Memory Polymers for Smart Structures," *Composites Part B: Engineering* 248 (2023): 110382.

141. D. Rahmatabadi, K. Mirasadi, A. Bayati, et al., "4D Printing Thermo-Magneto-Responsive PETG-Fe_3O_4 Nanocomposites With Enhanced Shape Memory Effects," *Applied Materials Today* 40 (2024): 102361.

142. Y. Li, Z. Li, Q. Wang, et al., "3D-Printed Magnetic Porous Structures With Different Poisson's Ratios and Their Mechanoelectrical Conversion Capabilities," *Additive Manufacturing* 69 (2023): 103542.

143. S. Zhang, Y. Xu, Z. Li, et al., "Ultra-Fast Shape-Deformation and Highly-Sensitive Detection of 4D Printed Electromagnetic Architectures," *Advanced Functional Materials* 34 (2024): 2402563.

144. X. Chen, P. Chen, J. Shi, et al., "Hybrid 3D Printing of Continuous Carbon Fiber Magneto-Electric Composites for Load Real-Time Sensing and Energy Absorption," *Advanced Functional Materials* 35 (2025): 2425794.

145. H. Ceylan, I. C. Yasa, O. Yasa, A. F. Tabak, J. Giltinan, and M. Sitti, "3D-Printed Biodegradable Microswimmer for Theranostic Cargo Delivery and Release," *ACS Nano* 13 (2019): 3353–3362.

146. X. Wang, X. H. Qin, C. Hu, et al., "3D Printed Enzymatically Biodegradable Soft Helical Microswimmers," *Advanced Functional Materials* 28 (2018): 1804107.

147. I. C. Yasa, A. F. Tabak, O. Yasa, H. Ceylan, and M. Sitti, "3D-Printed Microrobotic Transporters With Recapitulated Stem Cell Niche for Programmable and Active Cell Delivery," *Advanced Functional Materials* 29 (2019): 1808992.

148. F. Li, S.-F. Liu, W. Liu, et al., "3D Printing of Inorganic Nanomaterials by Photochemically Bonding Colloidal Nanocrystals," *Science* 381 (2023): 1468–1474.

149. J. Li, J. Cao, R. Bian, et al., "Multimaterial Cryogenic Printing of Three-Dimensional Soft Hydrogel Machines," *Nature Communications* 16 (2025): 185.

150. Y. Zhang, C. Pan, P. Liu, et al., "Coaxially Printed Magnetic Mechanical Electrical Hybrid Structures With Actuation and Sensing Functionalities," *Nature Communications* 14 (2023): 4428.

151. Z. Liu, Y. Zhang, J. Cai, et al., "Soft-Hard Magnetic Transformable Coaxial Fiber With Multimodal Deformations," *Advanced Functional Materials* 35 (2025): 2421254.

152. J. H. Hwang, S. Won, J. M. Lee, et al., "Closed-Loop and Sustainable 4D Printing of Multi-Stimuli-Responsive Sulfur-Rich Polymer Composites for Autonomous Task Execution," *Advanced Materials* 37 (2025): 07057.

153. G. Chung, H. L. Quang, J. H. Kim, J. Yoo, S. K. Seol, and Y. Park, "Bioinspired, Rapidly Responsive Magnetically Tunable Stiffness Metamaterials," *Advanced Materials* 37 (2025): 2505880.

154. J. Simińska-Stanny, M. Nizioł, P. Szymczyk-Ziółkowska, et al., "4D Printing of Patterned Multimaterial Magnetic Hydrogel Actuators," *Additive Manufacturing* 49 (2022): 102506.

155. Y. Wang, H. Zhu, X. Ye, et al., "4D Printing of Magneto-and Thermo-Responsive, Adaptive and Multimodal Soft Robots," *Virtual and Physical Prototyping* 20 (2025): 2457025.

156. X. Ou, Y. Sheng, J. Huang, et al., "3D Printed Swordfish-Like Wireless Millirobot," *Advanced Intelligent Systems* 7 (2025): 2400206.

157. S. Roh, L. B. Okello, N. Golbasi, et al., "3D-Printed Silicone Soft Architectures With Programmed Magneto-Capillary Reconfiguration," *Advanced Materials Technologies* 4 (2019): 1800528.

158. Z. Li, J. Dong, S. Zhang, et al., "Phase Transition Reversible 3D Printing of Magnetic Thixotropic Fluid," *Applied Materials Today* 34 (2023): 101920.

159. G. Shao, H. O. T. Ware, J. Huang, R. Hai, L. Li, and C. Sun, "3D Printed Magnetically-Actuating Micro-Gripper Operates in Air and Water," *Additive Manufacturing* 38 (2021): 101834.

160. G. Shao, H. O. T. Ware, L. Li, and C. Sun, "Rapid 3D Printing Magnetically Active Microstructures With High Solid Loading," *Advanced Engineering Materials* 22 (2020): 1900911.

161. Z. Li, D. Weng, L. Chen, Y. Ma, Z. Wang, and J. Wang, "Precision 3D Printing of Strongly Magnetic Soft Structures Containing High Concentrations of NdFeB," *Applied Materials Today* 42 (2025): 102610.

162. S. Lee, D. Park, Y. Cho, and J. Kim, "Vertically-Aligned Boron Nitride Composite as a Highly Thermally Conductive Material Using Magnetic

Field-Assisted Three-Dimensional Printing," *Ceramics International* 49 (2023): 7050–7056.

163. S. Lantean, I. Roppolo, M. Sangermano, M. Hayoun, H. Dammak, and G. Rizza, "Programming the Microstructure of Magnetic Nanocomposites in DLP 3D Printing," *Additive Manufacturing* 47 (2021): 102343.

164. D. Kokkinis, M. Schaffner, and A. R. Studart, "Multimaterial Magnetically Assisted 3D Printing of Composite Materials," *Nature Communications* 6 (2015): 8643.

165. C. Xu, P. Zhou, X. Zhou, L. Zhang, Q. Liu, and L. Ren, "Magnetically Assisted Direct Writing 3D Printing Programmable Magnetically Responsive Origami Actuator," *Additive Manufacturing* 109 (2025): 104898.

166. C. Ma, S. Wu, Q. Ze, et al., "Magnetic Multimaterial Printing for Multimodal Shape Transformation With Tunable Properties and Shiftable Mechanical Behaviors," *ACS Applied Materials & Interfaces* 13 (2021): 12639–12648.

167. C. Wang, Z. Zhao, Z. Li, Y. Jia, A. A. Sharma, and X. S. Zhang, "Direct Ink Writing of Magnetic Soft Materials With Optimized Printing Path," *Additive Manufacturing* 105 (2025): 104770.

168. Z. Ma, Y. Wu, S. Lu, et al., "Magnetically Assisted 3D Printing of Ultra-Antiwear Flexible Sensor," *Advanced Functional Materials* 34 (2024): 2406108.

169. A. Pardo, S. M. Bakht, M. Gomez-Florit, et al., "Magnetically-Assisted 3D Bioprinting of Anisotropic Tissue-Mimetic Constructs," *Advanced Functional Materials* 32 (2022): 2208940.

170. J. J. Martin, B. E. Fiore, and R. M. Erb, "Designing Bioinspired Composite Reinforcement Architectures via 3D Magnetic Printing," *Nature Communications* 6 (2015): 8641.

171. H. Sun, C. Zhang, C. Pan, et al., "Magnetic Field-Assisted Manufacturing of Groove-Structured Flexible Actuators With Enhanced Performance," *Additive Manufacturing* 80 (2024): 103979.

172. Z. Li, Y. P. Lai, and E. Diller, "3D Printing of Multilayer Magnetic Miniature Soft Robots With Programmable Magnetization," *Advanced Intelligent Systems* 6 (2024): 2300052.

173. E. B. Joyee, A. Szmelter, D. Eddington, and Y. Pan, "3D Printed Biomimetic Soft Robot With Multimodal Locomotion and Multifunctionality," *Soft Robotics* 9 (2022): 1.

174. X. Li, W. Shan, Y. Yang, et al., "Limpet Tooth-Inspired Painless Microneedles Fabricated by Magnetic Field-Assisted 3D Printing," *Advanced Functional Materials* 31 (2021): 2003725.

175. P. Wu, T. Yu, and M. Chen, "Magnetically-Assisted Digital Light Processing 4D Printing of Flexible Anisotropic Soft-Magnetic Composites," *Virtual and Physical Prototyping* 18 (2023): 2244924.

176. P. Wu, T. Yu, M. Chen, N. Kang, and M. E. Mansori, "Electrically/Magnetically Dual-Driven Shape Memory Composites Fabricated by Multi-Material Magnetic Field-Assisted 4D Printing," *Advanced Functional Materials* 34 (2024): 2314854.

177. H. Wang, Y. Zhang, X. Liu, et al., "Stable Magnetic Soft Structures," *Science Advances* 11 (2025): adz4952.

178. X. Sun, L. Yue, L. Yu, et al., "Machine Learning-Enabled Forward Prediction and Inverse Design of 4D-Printed Active Plates," *Nature Communications* 15 (2024): 5509.

179. Z. Liu, M. Li, X. Dong, Z. Ren, W. Hu, and M. Sitti, "Creating Three-Dimensional Magnetic Functional Microdevices via Molding-Integrated Direct Laser Writing," *Nature Communications* 13 (2022): 2016.

180. H. Deng, K. Sattari, Y. Xie, P. Liao, Z. Yan, and J. Lin, "Laser Reprogramming Magnetic Anisotropy in Soft Composites for Reconfigurable 3D Shaping," *Nature Communications* 11 (2020): 6325.

181. Q. Deng, H. Li, H. Zhu, et al., "Spatiotemporal Modulation of Magnetization in Magnetic Soft Materials," *Advanced Materials* 37 (2025): 06342.